CSIRO LAND AND WATER
www.csiro.au

Ground displacements over alluvial aquifers in Southern Inland New South Wales

24 December 2021

Report prepared for The New South Wales Department of Planning, Industry & Environment

NSW GOVERNMENT | Planning, Industry & Environment

Acknowledgements

We acknowledge the partnership with the New South Wales Department of Planning, Industry & Environment (NSW DPIE) Water Group (in Prem Kumar). We also thank the NSW DPIE Water Group for sharing data and technical assistance.

Citation

Castellazzi P[1], Schmid W[2], and Fu G[2] (2021) Ground displacements over alluvial aquifers in Southern Inland New South Wales.

[1]CSIRO Land and Water, Urrbrae, SA

[2]CSIRO Land and Water, Floreat, WA

Copyright

© Commonwealth Scientific and Industrial Research Organisation 2021. To the extent permitted by law, all rights are reserved and no part of this publication covered by copyright may be reproduced or copied in any form or by any means except with the written permission of CSIRO.

Important disclaimer

CSIRO advises that the information contained in this publication comprises general statements based on scientific research. The reader is advised and needs to be aware that such information may be incomplete or unable to be used in any specific situation. No reliance or actions must therefore be made on that information without seeking prior expert professional, scientific and technical advice. To the extent permitted by law, CSIRO (including its employees and consultants) excludes all liability to any person for any consequences, including but not limited to all losses, damages, costs, expenses and any other compensation, arising directly or indirectly from using this publication (in part or in whole) and any information or material contained in it.

CSIRO is committed to providing web accessible content wherever possible. If you are having difficulties with accessing this document please contact csiroenquiries@csiro.au.

Contents

Figures

Tables

Executive summary

The NSW Department of Planning, Industry & Environment (NSW-DPIE), as a regulatory agency, is concerned about ground deformation in alluvial groundwater sources in southern inland New South Wales particularly if it is the result of irreversible, inelastic compaction that follows dewatering (NSW, 2021b). The NSW Water Management Act 2000 (WMA, 2000) and the water sharing plans for alluvial groundwater sources allow for the prevention of structural damage to aquifers of the groundwater sources resulting from groundwater extraction.

Therefore, the aim is not only to map ground deformation over seven aquifers of Southern Inland NSW (corresponding to seven NSW-DPIE groundwater sources), but also to determine the impact that dewatering-induced inelastic aquifer compaction and groundwater-oscillation induced elastic compaction or expansion as well as any other controlling factors, such as screen depth, aquifer layers, land cover, terrain, soil clay and moisture content, as well as rivers and flood plains.

NSW-DPIE has commissioned CSIRO to undertake the present study, which comprises three phases: (1) creating large-scale deformation maps from radar interferometry, a technique using spaceborne radar images to track satellite-to-ground distance changes; (2) exploring the temporal correlations between ground displacement time-series and groundwater head time-series; (3) exploring how machine learning can help us interpret the controlling factors of the spatially variable correlations between ground displacement time-series and groundwater head time-series.

A ground deformation map is produced for the period from late-2015 to mid-2020 and shows deformation below detection threshold over most of the study area. However, some low-amplitude anomalies are detected, and their spatial patterns, along with knowledge of the location of groundwater extraction areas, allow a first judgment on their potential relation to groundwater factors. Four of these anomalies are potentially correlated with groundwater, given their proximity to groundwater extraction bores used for irrigation, and given the temporal correlations of groundwater vs. ground level changes: (1) the eastern Lower Murrumbidgee and (2) the eastern Lower Lachlan groundwater sources (within Calivil Formation and Renmark Group), along the river corridors of (3) the Upper Lachlan and (4) Upper Murray in groundwater sources (within Cowra/Shepparton and Lachlan formations).

A machine-learning approach is used to infer the spatial variability of the correlation between groundwater head and ground deformation from 18 explanatory variables divided into four sub-categories, each explaining potential contributions to this correlation: surficial factors of deformation such as clayey soil and changes in moisture, ground deformation measurement noise, terrain factors (slope, elevation etc.) and groundwater factors. An inherent drawback of the method is that the unbalanced proportions of contributors lead to unbalanced results, where the groundwater contributors are necessarily underestimated given the lack of lithological paraments in the model. Such compressibility and thickness parameters are essential to describe the potential for groundwater-related ground deformation. Nevertheless, a good model can be produced with the data that are available, which proves the particular attention to surficial soil factors such as clay content in the interpretation of groundwater-related deformation. InSAR noise is also a strong contributing factor, although unavoidable at this time given the nature of radar

data that are available across the study area. Newer radar missions will contribute to solve that limitation in the near future.

Recommendations for future work are, firstly, to improve the relation between ground deformation and groundwater and, secondly, to better allocate ground deformation data to other influential factors.

The improvement of the relation between ground deformation and groundwater includes the placement of corner reflectors over locations where ground deformation and groundwater levels are highly correlated to increase to precision of ground deformation data and prevent most of the noise from surficial clays. Furthermore, “child” Rand Forest analyses could be designed for certain areas where a compilation of consistent lithological information is available on the scale of groundwater sources or even, on a more local scale, on the basis of piezometer-clusters that show similar strong positive temporal correlation between critical heads and InSAR deformation.

A better allocation of ground deformation data to other influential factors includes, firstly, the comparison of SBAS-InSAR ground deformation data influenced by surficial clays with InSAR analysis targeted on highly coherent radar targets unaffected by surficial clays and, secondly, the measurement of in-situ the surficial ground deformation and its relation to moisture and cropping cycles.

Introduction

The Water Sharing Plans for the NSW Groundwater Sources include an objective to "contribute to the prevention of structural damage to aquifers of the alluvial groundwater sources resulting from groundwater extraction" (Part 2, Section 9(2c)) (NSW, 2021b). In addition, the risk assessments for groundwater resource plans undertaken to meet New South Wales's obligations of the Murray-Darling Basin Plan (NSW, 2021a) identified induced sediment compaction as a major data gap to manage the long-term integrity of the alluvial groundwater sources in NSW.

Structural damage to an aquifer includes any permanent compaction of sediments within the groundwater sources, resulting from depressurisation or dewatering (NSW, 2021b). Consequently, it is of interest for the regulatory agency, the New South Wales Department of Planning, Industry & Environment (NSW-DPIE) to not only assess ground deformation, but also to determine whether it is the result of irreversible, inelastic compaction that follows dewatering. This information is particularly useful for water level response management and as decision-support basis for implementing any restrictions on groundwater extractions necessary to 'prevent land subsidence or compaction in an aquifer' as required under the NSW Water Management Act 2000 (WMA,2000).

Therefore, NSW-DPIE commissioned CSIRO to explore the potential of land subsidence in groundwater sources in southern inland New South Wales, where significant groundwater extraction is occurring. This work is an extension of a previous analysis of ground displacement in the Lower Namoi Groundwater Source (Castellazzi and Schmid, 2020), where CSIRO completed an analysis of displacement derived from space-borne radar imagery (Interferometric Synthetic Aperture Radar (InSAR) with correlation of survey benchmarks and groundwater level hydrographs as well as soils and land use.

The objectives of this study are firstly to derive recent ground displacement from InSAR in the alluvial groundwater sources in southern inland NSW located in the southern part of the Murray-Darling Basin. Secondly, the study aims to correlate the deformation with groundwater level information in order to determine where in space and at which aquifer depths extraction could have led to inelastic compaction. However, southern inland NSW is not only characterised by areas of irrigated agriculture with significant groundwater extraction but also by areas that are dominated by other surface factors that may have an impact on ground deformation such as variable land use, soil clay content, influence of rivers and flood plains, and climate. Therefore, in this study, aside from groundwater-related parameters, several other contributing factors that can potentially influence the InSAR measurements and associated noise are investigated. For that, we employ a multi-factorial machine-learning technique called 'Random Forest" to assess a ranking of impact of all influential variables on InSAR deformation.

The study area encompasses three major groundwater sources in Southern Inland NSW and several smaller upstream groundwater sources: Lower and Upper Lachlan alluvial groundwater source (LL, UL), Lower and Mid Murrumbidgee alluvial groundwater sources (LMB, MMB) and Lower and Upper Murray alluvial groundwater sources as well as Billabong Creek Alluvial Groundwater Source (LM, UM, BC; Figure 1A).

To facilitate comprehension for the international science community, the term ʾAquiferʿ will be used in place of ʾGroundwater sourceʾ, as commonly used and defined by NSW-DPIE, thereafter and throughout the report. The term ʾAquifer layerʾ, however, refers to a specific lithological unit typically defined as an aquifer or a hydrogeological formation, i.e. a body of rock and/or sediment that holds groundwater.

To cover the study area, two Sentinel-1 swaths were used and merged (Figure 1B). The two swaths used for InSAR processing cover an area of approximately 450 km by 450 km.

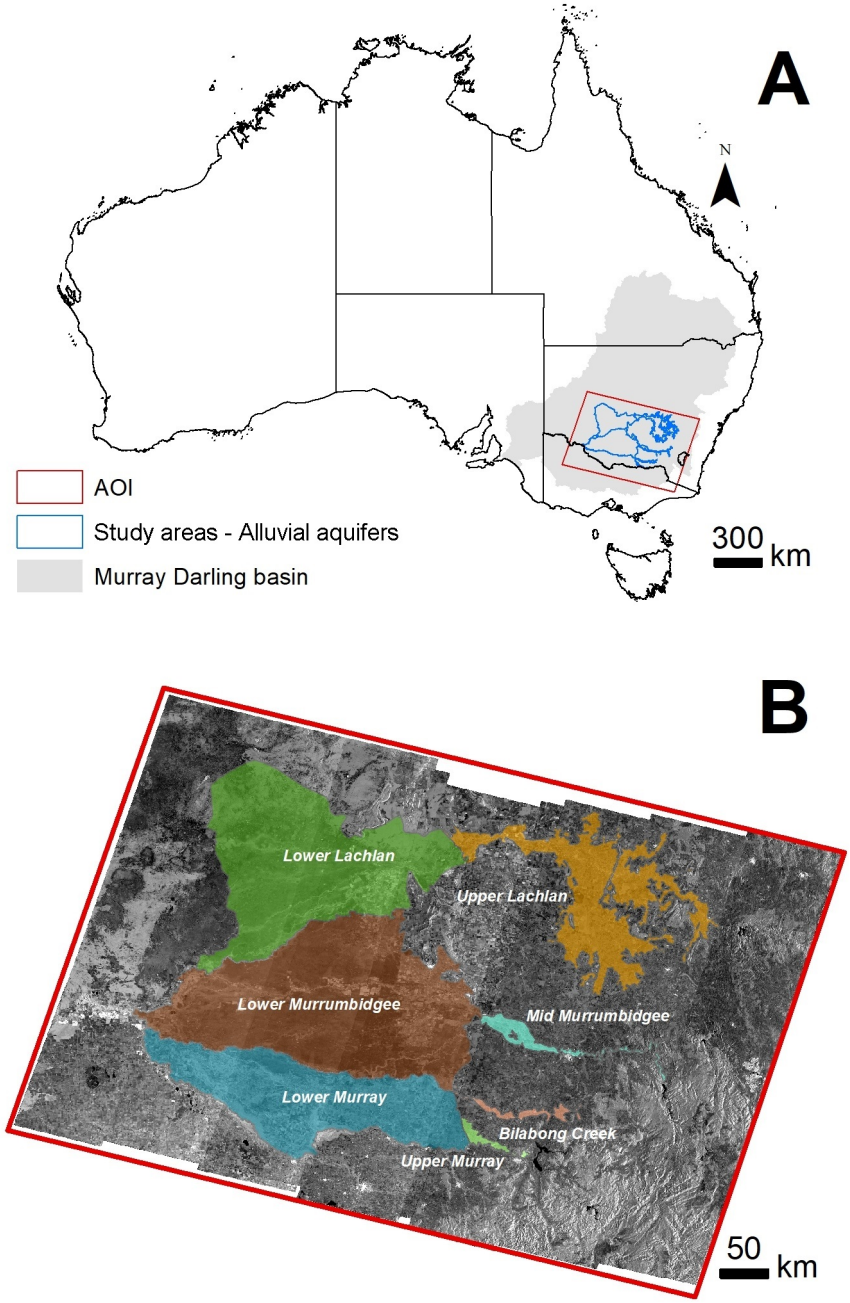

Figure 1 Location of study area and of the Area Of Interest (AOI; part A) considered for ground deformation mapping, with boundaries of the seven aquifers overlaid on Sentinel-1 radar images (part B).

Part I Measuring ground displacements

Radar interferometry, or InSAR, uses the phase observations of a Synthetic Aperture Radar (SAR) sensor to retrieve information about the distance change between the sensor's antenna and the ground. By using radar image time series acquired from the same orbital position, the distance chance can be interpreted as a modification of the ground level.

The InSAR technique has been optimized for numerous applications, including volcano monitoring, landslide risk assessment, monitoring of fault movements and earthquakes, and subsidence due to groundwater depletion. One major challenge related to using InSAR to retrieve groundwater-related ground deformation over a large regional area is interpreting the phase where it is of low or medium quality (Castellazzi and Schmid, 2021), i.e., where it is of low quality and/or affected by numerous factors different from the signal to be retrieved. As technical details of InSAR processing were discussed in detail during a previous, similar project, we invite interested readers to read the related report (Castellazzi and Schmid, 2020).

1 Radar imagery

Sentinel-1 data are acquired along 250 km-wide swaths covering all continents at least every 12 days. Three swaths are required to cover the study area, as shown by Figure 2, and a 50 km-wide overlap exists in between each swath. All swaths were acquired during descending orbits, with the satellite flying east of the study and its antennas oriented to the right. The three swaths used in this study are referred to as Western, Central and Eastern swaths hereafter. For each swath, time-series of 132 acquisitions all acquired from late-2015 to mid-2020 were downloaded from The Sentinel Australasia Regional Access (SARA) web portal. Due to the swath length required from each swath (>500km) and the archiving format of Sentinel-1 data, two to three tiles were required to cover each acquisition date for each swath.

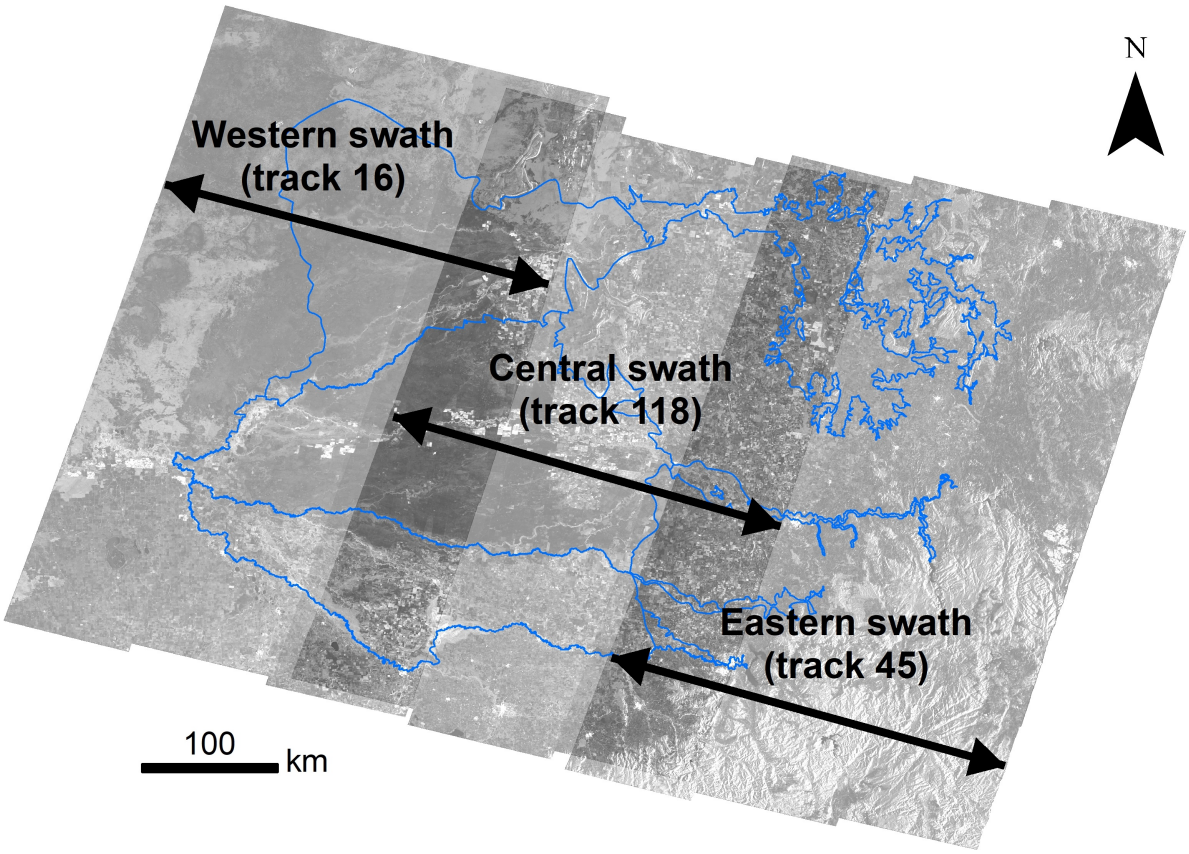

Figure 2 Coverage and overlap area of the three Sentinel-1 swaths used to produce the vertical ground deformation map.

Table 1 Main characteristics of the three stacks of SAR images used in this study

	Orbital track number/orientation	Number of images	Number of interferograms	Start/End dates
Eastern swath	45/Descending	132	592	20151027 20200427
Central swath	118/Descending	132	580	20151101 20200502
Western swath	16/Descending	132	571	20151106 20200531

2 InSAR processing

Based on the three radar image time series, three connection graphs were produced (Figure 3), allowing to visualize the image pairs and phase shift maps (interferograms) to produce for each InSAR processing to from the three interferogram stacks. The three interferogram stacks are then converted to displacements during the interferogram stacking (inversion) steps. We note that all connection graphs not only comprise the same number of images but are also relatively similar in terms of design (Figure 3; Table 1). This, along with similar processing parameters for each swath (Figure 4) allows to produce three deformation time-series with comparable precision and noise level, which helps interpretation.

InSAR processing parameters are shown on Table 2. They were set based on previous experience for InSAR processing over similar land use settings (Castellazzi and Schmid, 2021). The InSAR processing strategy is the Intermittent Small Baseline Subset-InSAR, or ISBAS-InSAR (Berardino et al., 2002; Sowter et al., 2013). This strategy allows close-to-complete coverage over low or sparse vegetation settings, typical of groundwater irrigation areas. This coverage is provided at the cost of a spatially variable noise level (e.g., between pixels of the same swath), depending on the temporal stability of the radar signal along the radar acquisition time series. All results from InSAR processing provide information on the satellite Line-Of-Sight (LOS) distance change, i.e., InSAR measures deformation along a non-vertical axis. We reprojected the deformation values along a vertical axis by assuming the horizontal component of deformation negligible.

The three vertical ground deformation data cubes resulting from the InSAR processing (multitemporal maps) were postprocessed in order to cover the whole study area with a single deformation data cube. In order for all deformation time-series to correspond to the same time vector, the two most eastern swath were temporally resampled using a linear interpolation algorithm (resample function in MATLAB 2018). The time vector used for resampling comprises only the temporal period in common for all InSAR time series and respects the original time stepping of the most eastern swath. Average values were computed for pixels covered by the two swaths. A least-square linear fitting algorithm was used to compute a mean vertical velocity map in mm/yr for the whole study period and for individual years.

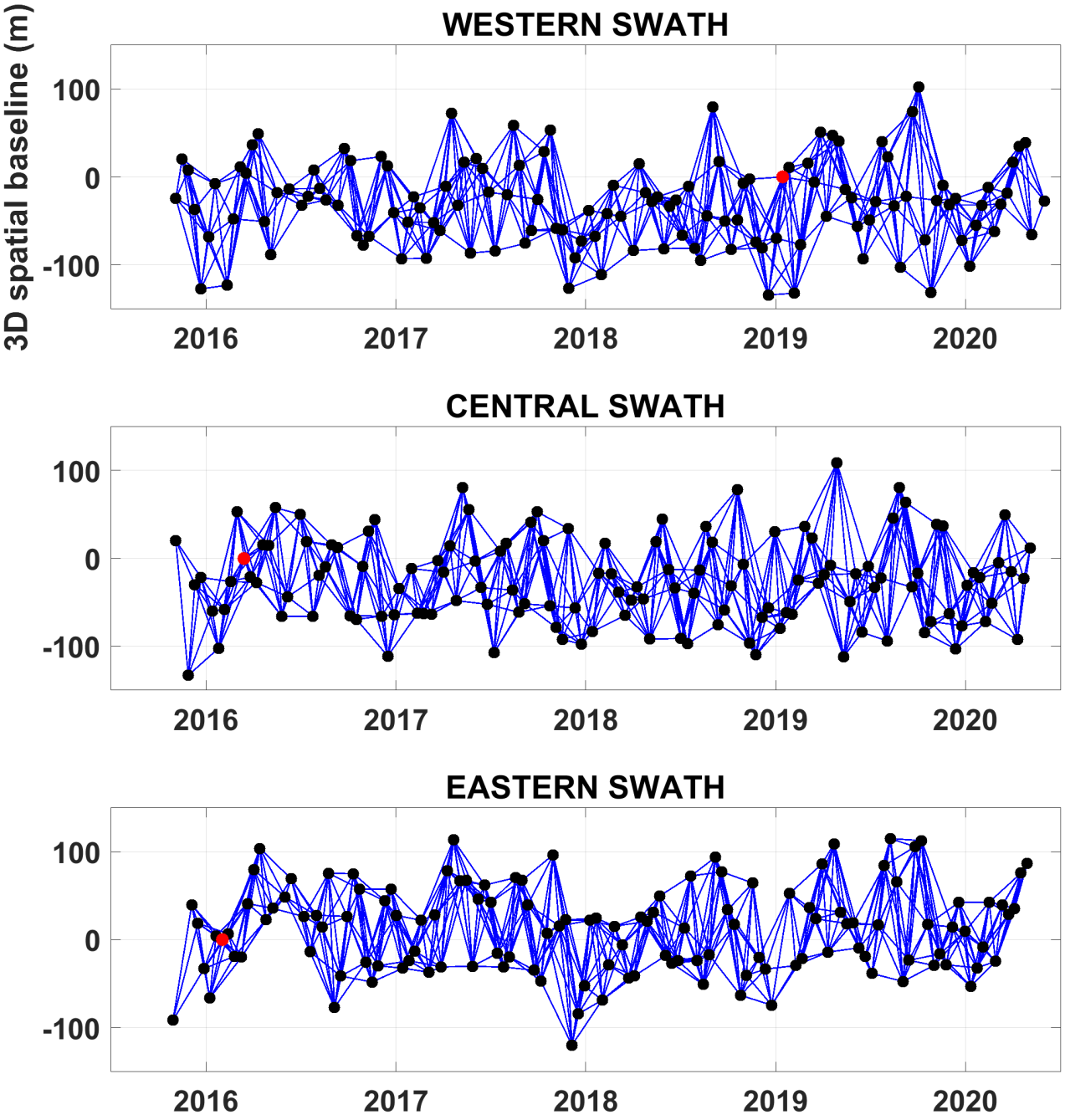

Figure 3 Connection graphs used to generate interferogram stacks from the two time-series of SAR images. The graphs represent the moment (x axis) and positioning (y axis) in reference to the master image (red point). Each black point corresponds to an image, and each blue line represents an interferogram.

Table 2 Main parameters of the InSAR processing.

Parameter	Setting
Look factor	Range 42; Azimuth 11
Filtering	Goldstein adaptative to coherence – alpha range [0.3; 2]
Flattening	Fitting with polynomial of degree 5 for each interferogram, fitting with polynomial of degree 2 for the final displacement maps.
Digital Elevation Model for topographic corrections	ALOS-3D DEM version 3.1, Tadono et al., 2016
Phase to displacement Inversion method	ISBAS implemented in SARSCAPE 5.5 (version 5.5.4), Jacobi SVD. Inversion weighed to coherence.
Pixel selection criteria	Spatial coherence mask: 0.20 Minimum percentage of valid Interferograms: 50 % Minimum percentage of valid images: 65 % (missing dates are interpolated) Temporal coherence mask: 0.25
Atmospheric filtering	Low-pass filter of 1200 m, High-pass filter of 120 days
Coherence computation	5 x 5 kernel
Final spatial resolution	160 m

3 Results

The results of the InSAR processing and postprocessing are presented in Figure 4. While the InSAR deformation map alone does not allow to properly locate deformation signals, the overlay with radar intensity maps allows locating major landscape and geomorphological features such as rivers and agricultural areas. No deformation data have bene retrieved in and around the Australian Alps (Southeast corner, Figure 4) due to low coherence related to dense vegetation and high topographic gradients. Preliminary findings are that InSAR detects no deformation for most of the study area, with values mostly in the range [-10; 10] mm/yr, aside from few anomalies beyond this range. This range is slightly narrower than the detection threshold obtained by Castellazzi and Schmid (2021) but can be considered as a reasonable range below detection threshold given the land use setting.

Several anomalies will be discussed with more details in the subsequent sections. It is important to note that the spatial pattern of an anomaly is crucial for interpretation and allocation of the signal to a specific phenomenon. For example, while the Murray catchment presents a spatially distributed uplift signal, it is not spatially continuous and follows agricultural boundaries, suggesting that the signal is related to a series of surficial soil deformations and agricultural activities. Two main, low amplitude, negative deformation areas (land subsidence) are potentially attributable to groundwater extraction. First, the Darlington Point area (Figure 4a), also encompassing the Coleambally area (LMB groundwater source) shows subsidence rates in the range [-10; -30] mm/yr. Second, The Hillston area (Lower Lachlan groundwater source; Figure 4b) show rates of similar amplitude. Given the low amplitude of the deformation and its spatial patterns not clearly coinciding with any obvious geomorphological or lithological boundaries, allocating the deformation to specific phenomena (e.g., groundwater depletion and storage, surface water and flooding, agricultural activities, soil clay content, climate variations to name a few) will require analysing deformation time-series with more details.

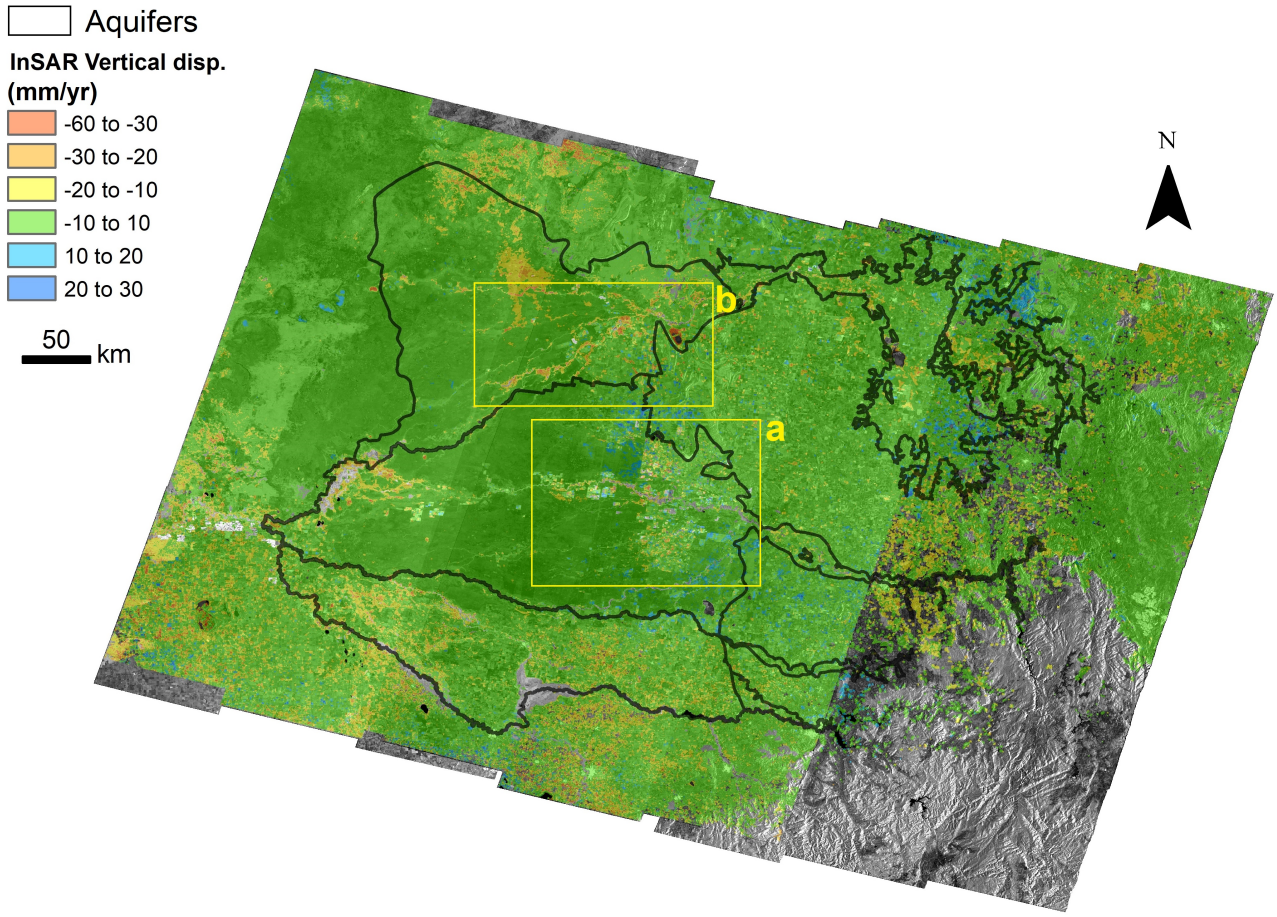

Figure 4 Mean vertical velocity map for the study area overlaid on a radar intensity map for clarity. Boundaries of the alluvial aquifers are also presented for spatial reference.

Figure 5 presents two North-South and West-East transects of mean vertical velocity for the entire study period. The North-South transect cuts the study area through the middle and shows values in the range [-20 +15] mm/yr. Three areas of negative values are observed, one in the Hillston area (Lower Lachlan aquifer), one in the Darlington Point area (Lower Murrumbidgee aquifer), and one in the most southern section of the study area in the Lower Lachlan aquifer. The West-East transects also cut the study area through the middle, and shows variations of the same amplitude,

i.e. [-20 +15] mm/yr. Three major observations can be drawn from that transect: (1) the presence of an area of negative deformation values (subsidence) in the most western portion of the study area; (2) an area of ample variations in the range [+5 -15] mm/yr in the central portion of the study area; (3) an area of negative to positive transition at the overlap of the central and eastern swath. While the negative values related to (1) do not seem to spatially match with any major groundwater abstraction area, and the one related to (3) seems related to the transition between two InSAR swaths, which may induce errors and abrupt changes in some cases. The ample variations related to (2) coincides with an intense groundwater abstraction area and could potentially be related to groundwater storage change.

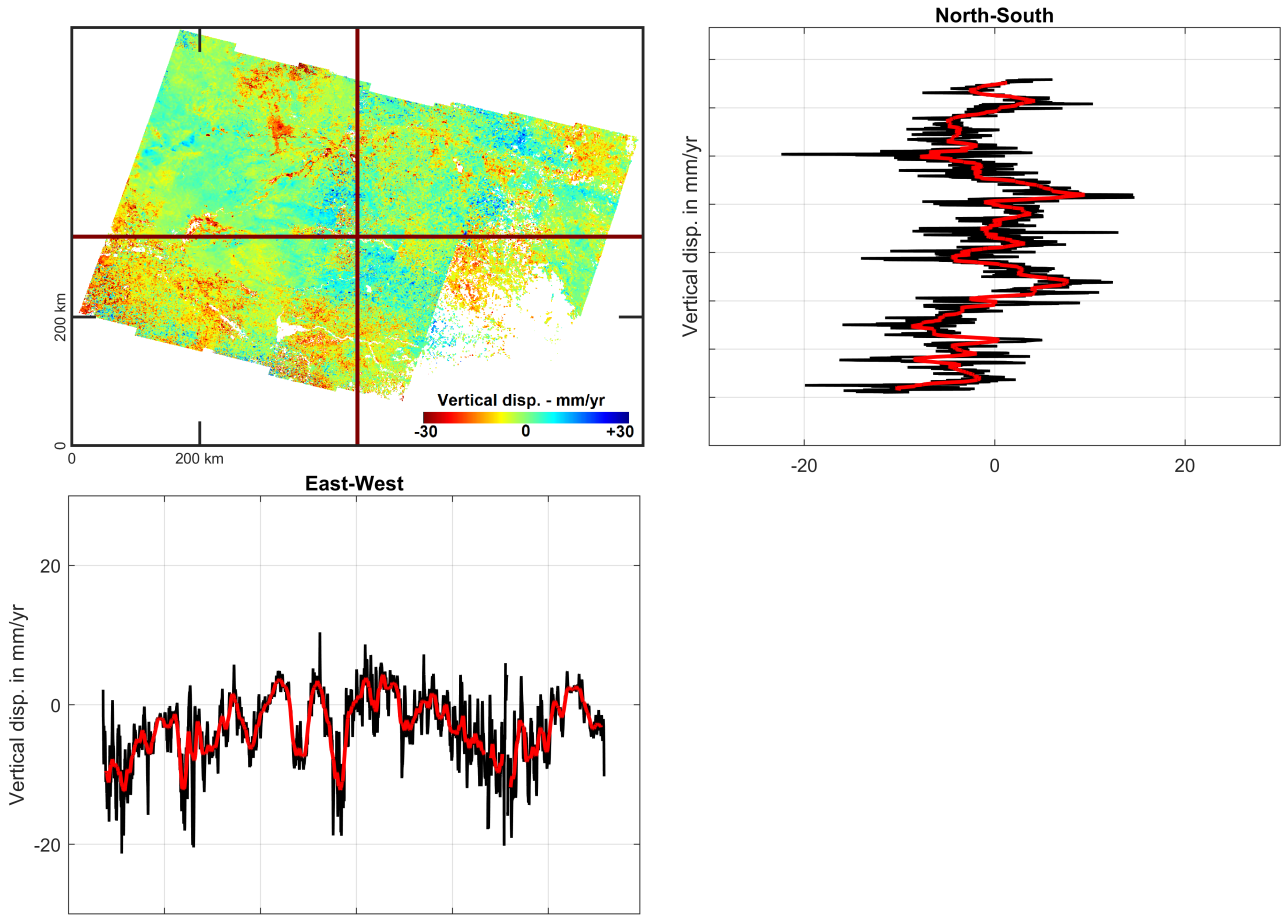

Figure 5 North-South and East-West transect of mean vertical deformation velocities for the study period (black lines), with a 10-km moving average filter (red line).

Figure 6 presents the mean annual deformation velocity, similar to Figure 4 and Figure 5, with a visualisation per aquifer. While most of the area is covered with deformation values below detection thresholds, within the [-10 +10] mm/yr interval, few anomalies can be observed. These anomalies are at the most eastern and western parts of the Lower Murrumbidgee aquifer, the eastern parts of the Lower Lachlan aquifer, and form a sparse signal throughout the Lower Murray. Signal variations in the range [-20 +20] mm/yr are observed in other aquifers, but no clear pattern is observed. By comparing the spatial patterns of deformation observed in Figure 4 and Figure 6 with the spatial distribution of the main groundwater production wells shown on Figure 7, we note that the two anomalies located in the eastern parts of the Lower Lachlan and Lower Murrumbidgee aquifers are potentially related to groundwater extraction. Given that such signal is also observed in other areas, where groundwater extraction does not occur, this spatial

coincidence is not sufficient to conclude on the influence of groundwater extraction on ground levels. It is important to note, however, that over the Darlington Point, Coleambally and Hillston areas, large groundwater drawdowns (change in pressure heads) or decline in recovered groundwater levels are observed.

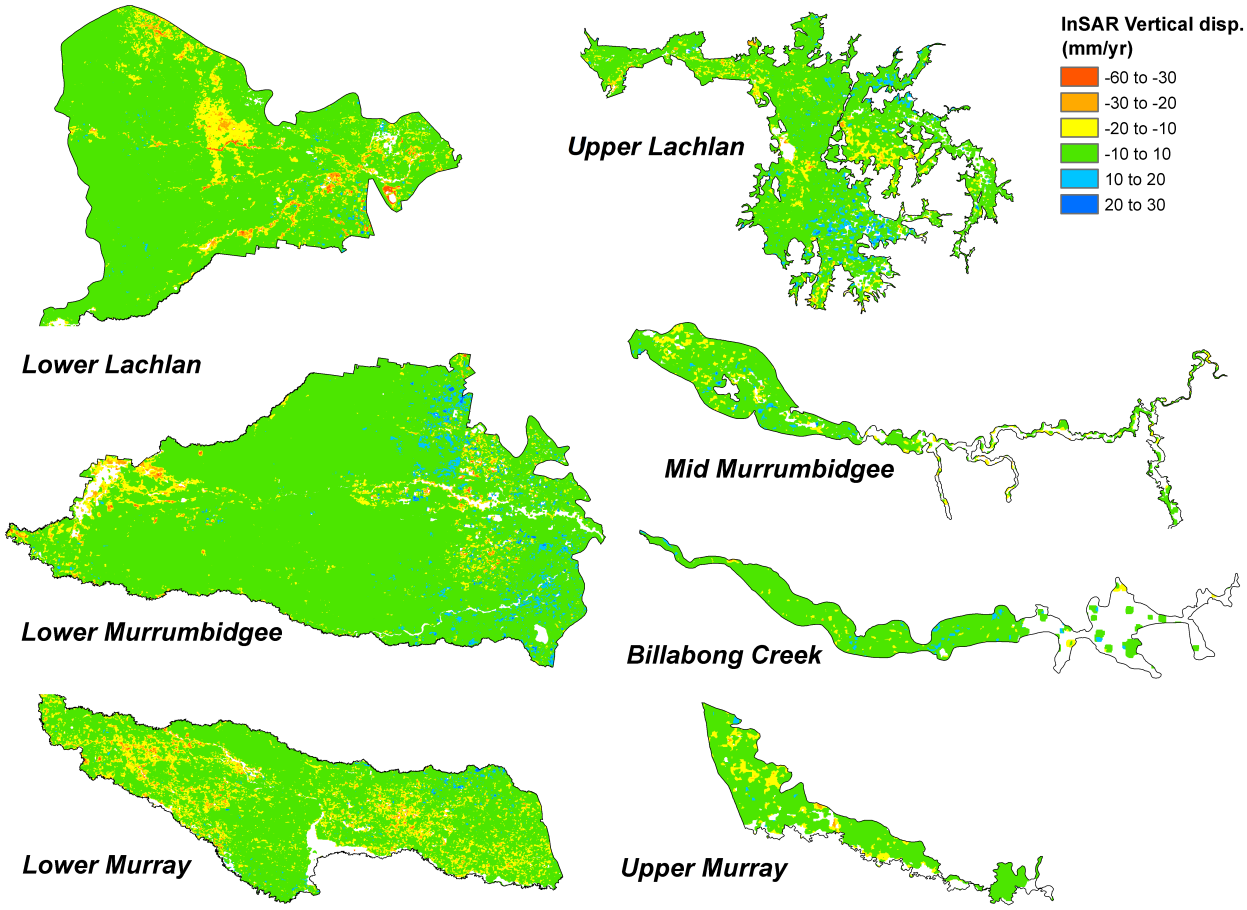

Figure 6 Vertical velocity of ground level changes for the seven aquifers (not drawn to scale).

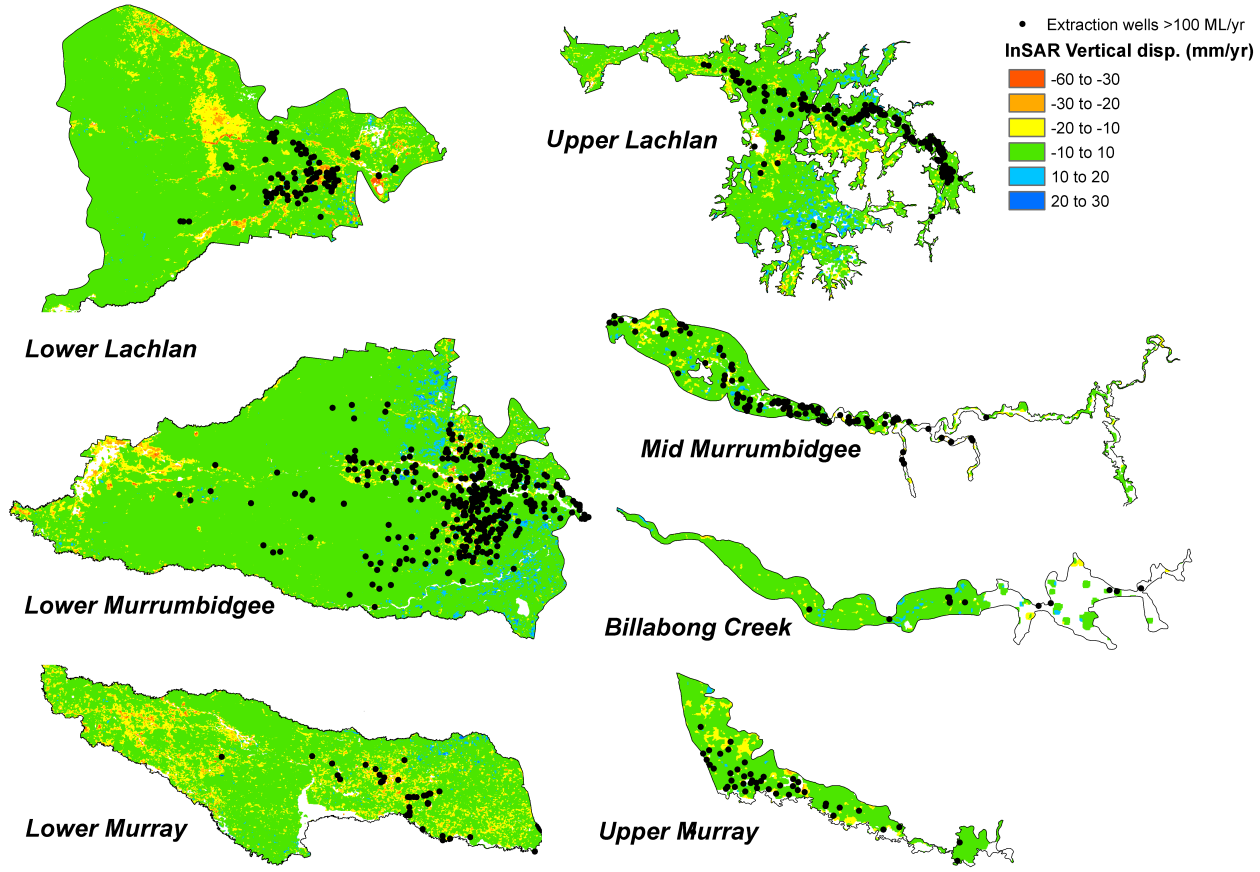

Figure 7 Vertical velocity of ground level changes for the seven aquifers, with locations of the wells with a maximal annual extraction higher than 100 ML/yr during the period 2015-2020 (not drawn to scale).

Part II Interpreting InSAR ground displacement data

The ISBAS-InSAR method used for this study pushes the limits of InSAR noise to provide close to full coverage over the study area. This is an unavoidable noise/coverage trade-off for InSAR performed from C-band (relatively short wavelength) radar data. Until longer wavelength radar images are available across Australia (L-band) with an acceptable temporal frequency, interpretation of InSAR ground deformation maps over regional Australia will require a multiple line of evidence approach.

This chapter explores the relation between InSAR ground deformation data and its potential contributors, whether they are related to groundwater or not, to support the interpretation of InSAR data for groundwater management purposes. The chapter is divided in three parts. First, we discuss the relations between InSAR data and potential influences unrelated to groundwater level changes, such as clayey soils and land use. Second, we explore and discuss the temporal correlations between groundwater levels and InSAR data. Third, we use a machine learning approach trained with a wide variety of potential contributors to the InSAR signal to explain the temporal relation between ground deformation data and groundwater levels.

4 InSAR signals unrelated to groundwater

4.1 Clay and moisture in surficial soils

Clayey soils shrink and expand with changes in moisture content. Also, climate variability is an important driving factor for soil moisture content of the uppermost soil horizons, hence such signal can affect short-term (from year-scale to decadal-scale) deformation products derived from InSAR, as observed in Castellazzi and Schmid (2020, 2021).

Figure 8 explores the relation between vertical InSAR deformation measurements and clay content for the first meter of soil for the two most western swaths. Unlike precedent studies over vertosols of the Lower Namoi groundwater source Castellazzi and Schmid (2020), no obvious relation can be found here. A subtle relation could be drawn for 2016 (given the shape of the scatter plot), which shows an increase of InSAR noise with increasing clay content up to 50%. However, another concurrent factor not directly related to clays, could explain such signal. As clays are preferentially deposited in depressions where temporary floods may occur, InSAR deformation values might be based upon less interferograms over these areas, making the InSAR measurements noisier. Again, as stated previously, in-depth analysis of influential factors will need to be carried to draw a robust interpretation of InSAR signals.

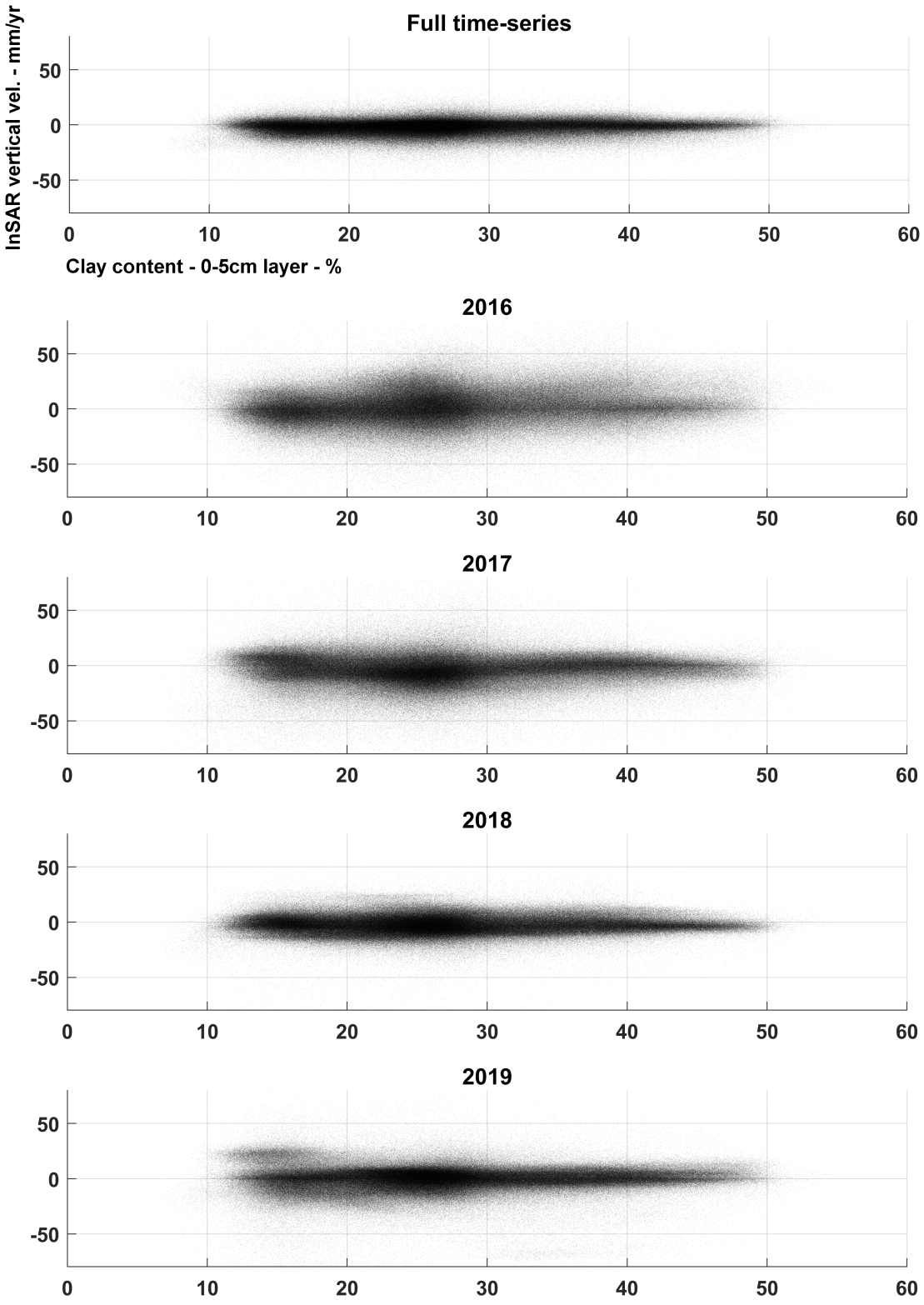

Figure 8 Relation between InSAR deformation (mm/yr) and the percentage of clay in the first five centimetres of soil (Viscarra Rossel et al., 2014).

Deformation maps for individual years of the InSAR period are shown in Figure 9. We note an important variability between years, showing distinct deformation rates and spatial patterns for each year. The year 2016 is dominated by large uplift areas across the Lower Lachlan aquifer and

in the eastern part of the Lower Murrumbidgee aquifer. The year 2017 shows uplift in the northern part of the Lower Lachlan and south of the Lower Murray aquifer. The year 2018 shows a generally stable ground surface, with a distinct subsidence pattern in the Lower Murrumbidgee aquifer, coinciding with the Darlington Point area. The year 2019 shows a distinct subsidence signal on the central/northern part of the Lower Lachlan aquifer (Willandra National Park), also visible on Figure 4. No interpretation is available for this signal at this stage, but the relation to groundwater is unlikely given the absence of major anthropogenic influence on groundwater resources in that area (Figure 7). Better clarity about influential factors is expected after correlating InSAR deformation with groundwater levels and several surface factors, such as clay content or land use.

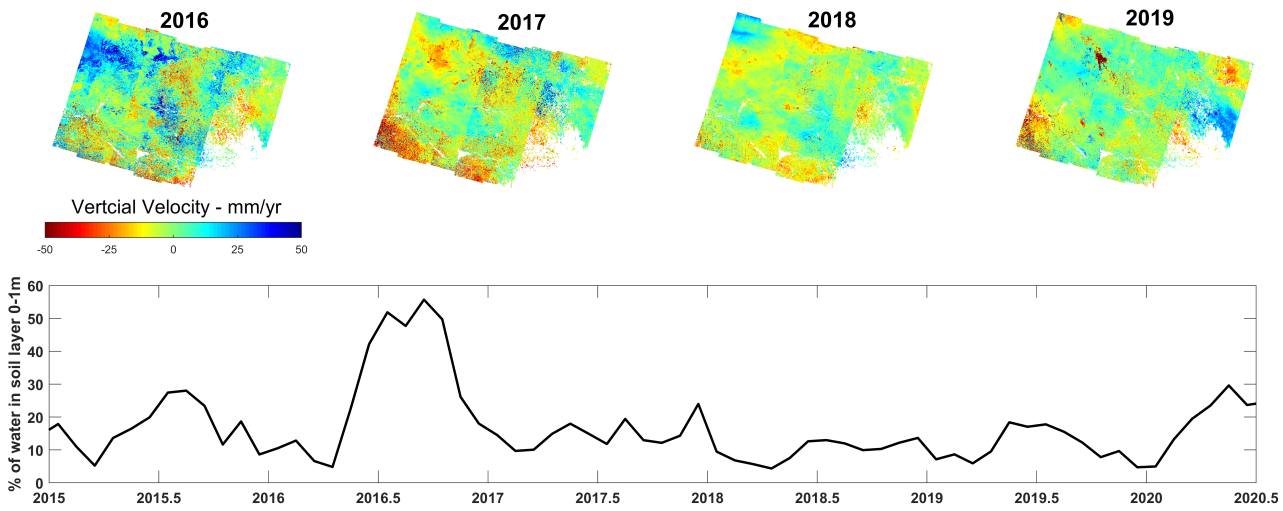

Figure 9 Mean annual vertical ground velocity for four years and corresponding soil moisture changes from The Australian Landscape Water Balance Model (AWRAv6; Frost et al., 2018).

4.2 Land use

Comparison between InSAR deformation and land use allows a first order assessment of factors influencing deformation and InSAR noise (Table 3). We note that the standard deviation in all major land use classes in the range [5.6; 8.8] mm/yr. Among these major land use classes, it is observed that 'irrigated cropping' areas show one of the most negative mean and median deformation values. While this observation suggests that groundwater is a driving factor of the measured deformation, we also note that land use classes for which standard deviation is high tend to show lower values of mean deformation (Figure 8).

Table 3 Land use classes and main statistics of InSAR vertical deformation signals. Land use classes representing more than 1% of the InSAR coverage are highlighted in grey.

Land use class	Mean	Median	Stdev.	% of the InSAR coverage	Mean % of coherent interferogram
2.1.0 Grazing native vegetation	-1.6	-0.9	5.6	52.1	86.5
3.3.0 Cropping	-0.5	-0.2	6.8	26.2	81.2
4.3.0 Irrigated cropping	-3.6	-3.4	8	7.5	74.3
1.1.0 Nature conservation	-3.7	-2.7	6.2	3.8	78.7
3.2.0 Grazing modified pastures	-1.3	-1.1	6.1	2.9	83.4
6.5.0 Marsh/wetland	0.1	0.2	5.7	1.9	88.3
1.3.0 Other minimal use	-2.3	-1.4	8.8	1.4	72.5
2.2.0 Production native forestry	-1	0.2	6.4	0.9	76.8
6.1.0 Lake	0.2	1.9	7.8	0.9	91.7
6.3.0 River	-4.8	-3.9	8	0.6	73.9
4.2.0 Grazing irrigated modified pastures	-4.3	-3.5	7.2	0.5	80.8
5.4.0 Residential and farm infrastructure	0.3	0.9	5.8	0.5	86.7
4.4.0 Irrigated perennial horticulture	-1.1	-0.1	6.8	0.3	73.4
5.7.0 Transport and communication	-0.3	-0.1	5.7	0.3	87
6.2.0 Reservoir/dam	-3.3	-2.2	7.6	0.1	76.3
6.4.0 Channel/aqueduct	-1.9	-1.3	7	0.1	77.1
1.2.0 Managed resource protection	-1.3	-1.4	6.7	0.1	77.3
5.5.0 Services	1.4	1.8	4.6	0.1	93.5
4.1.0 Irrigated plantation forests	-2.2	-2.5	6.7	0	65.9
4.5.0 Irrigated seasonal horticulture	-4.1	-3.6	7.2	0	70.5
4.6.0 Irrigated land in transition	-2.1	-2	5.5	0	75
3.4.0 Perennial horticulture	1.3	2.9	5.8	0	81.2
3.5.0 Seasonal horticulture	-6	-6.9	4.1	0	81.6
3.1.0 Plantation forests	0.2	1.3	7	0	81.9
5.2.0 Intensive animal production	-0.3	0.9	6.1	0	83.2
5.1.0 Intensive horticulture	0.1	1.5	4.9	0	85.9
5.9.0 Waste treatment and disposal	0.1	0.6	4.5	0	86.6
3.6.0 Land in transition	-0.5	-1.2	4.4	0	87.5
5.6.0 Utilities	0.9	0.4	5.2	0	89.2
5.8.0 Mining	-0.7	0	5.1	0	92.6
5.3.0 Manufacturing and industrial	2	2.5	3.9	0	96

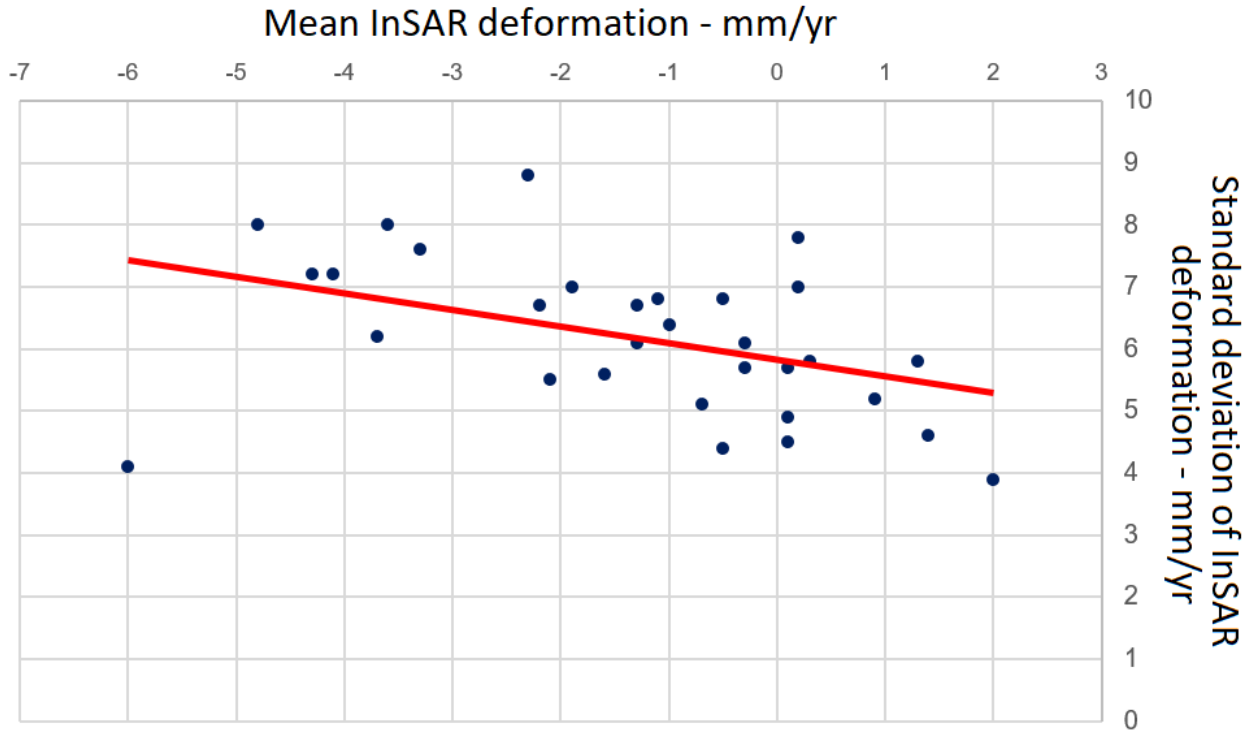

Figure 10 Mean InSAR deformation compared to standard deviation of InSAR deformation for each land use classes presented in Table 3.

5 Relation between groundwater and ground deformation

In order to study the inelastic effect of aquifer dewatering on deformation, the InSAR deformation can be compared with critical heads that represent the historical minimum of head level at which pre-consolidation occurred. Any water level fluctuation above those critical heads is assumed to solely influence elastic compaction and expansion. Any new drop of water levels to below previous critical heads established new critical heads and may impact inelastic subsidence.

Since regulatory concerns over irreversible, inelastic subsidence by far outweigh those over elastic, and hence reversible compaction and expansion, we firstly analyse the potential influence of critical heads on inelastic subsidence firstly before looking into whether head fluctuations may have an impact on elastic deformation.

It is important to note that the delay of the subsidence reaction is unaccounted in the analysis. For example, a sudden critical head drop followed by a quick recovery might not be sufficiently long to allow for full consolidation of compressible sediments. In this case, subsidence potentially occurs later if hydraulic head drops again down to historical minimum, even if the critical head stays.

5.1 Behaviour of critical heads and groundwater levels

In the LM, LMB, LL, and UL aquifers, significant drops in critical head to new consolidation levels can be observed since the beginning of water level record keeping. However, unlike in other parts of NSW, where these dewatering processes took place earlier (Lower Namoi between early 1980s to the mid-1990s: Castellazzi and Schmid, 2020), in the aquifers of southern inland NSW, periods with significant drops in critical head greater than 10 m occurred later within a period extending from the mid-1990s to late 2000s (Figure 11; Figure 12). This period of head decline coincides with the Millennium Drought. A renewed depletion commences in 2017 in the LL and LMB, most likely following increased pressure on groundwater abstraction during the recent drought from 2017-2019. The renewed drop in heads is the basis for the hypothesis that InSAR deformation within the InSAR observation period might be influenced by groundwater depletion. During that period, critical heads of most bores of the LM, UL, MMB, and UM do not drop below the minima established during the Millennium Drought.

The aim of displaying the horizontal and vertical distribution of the critical head drop of piezometers is to shed some light on specific aquifers or parts of aquifers that exhibit the most significant critical head drop. The hydrostratigraphy of the aquifers is conceptualised in existing groundwater models. NSW-DPIE provided information about hydrogeological layers of those models, which can be attributed to monitoring bores and also production bores. For simplicity, the layers were aggregated to Layer 1 (Cowra/Shepparton formations), Layer 2 (Calvil/Lachlan formations), Layer 3 (Renmark group), and Layer 4 (Cretaceous) (Table 4). Note that, according to NSW-DPIE, the bulk of the groundwater extractions generally occur in aggregated Layers 2 and 3.

Table 4 Aggregation of layers across different groundwater models

Aquifer	Model Layers	Formation in Groundwater Models	Aggregated Layers	Aggregated Formations
LM	1	Upper Shepparton Formation	1	Cowra/Shepparton
	2	Lower Shepparton Formation	1	Cowra/Shepparton
	3	Calivil Formation	2	Calvil/Lachlan
	4	Renmark Group	3	Renmark
LMB	1	Shepparton Fm	1	Cowra/Shepparton
	2	Calivil Fm	2	Calvil/Lachlan
	3	Renmark Fm	3	Renmark
LL	1	Shepparton Formation	1	Cowra/Shepparton
	2	Calivil Formation	2	Calvil/Lachlan
	3	Renmark Group	3	Renmark
	4	Cretaceous Sandstone	4	Cretaceaous
MMB	1	Cowra Fm	1	Cowra/Shepparton
	2	Lachlan Fm	2	Calvil/Lachlan
UM	1	Shepparton Formation	1	Cowra/Shepparton
	2	Lachlan Formation	2	Calvil/Lachlan
UL	1	Upper Cowra formation	1	Cowra/Shepparton
	2	Lower Cowra formation	1	Cowra/Shepparton
	3	Lachlan formation	2	Calvil/Lachlan

However, this layer attribution coming from multiple different groundwater model is, of course, somewhat subjective. In addition, for production bores where no GW number was present and/or no layer association could be made, assumptions were made by the client (e.g., Lower Lachlan: assigned to layers 2 and 3; Lower Murrumbidgee: deep production bores assigned to layers 1, 2, and 3; shallow production bores assigned to layer 1). Usage of production bores associated with multiple layers was prorated equally.

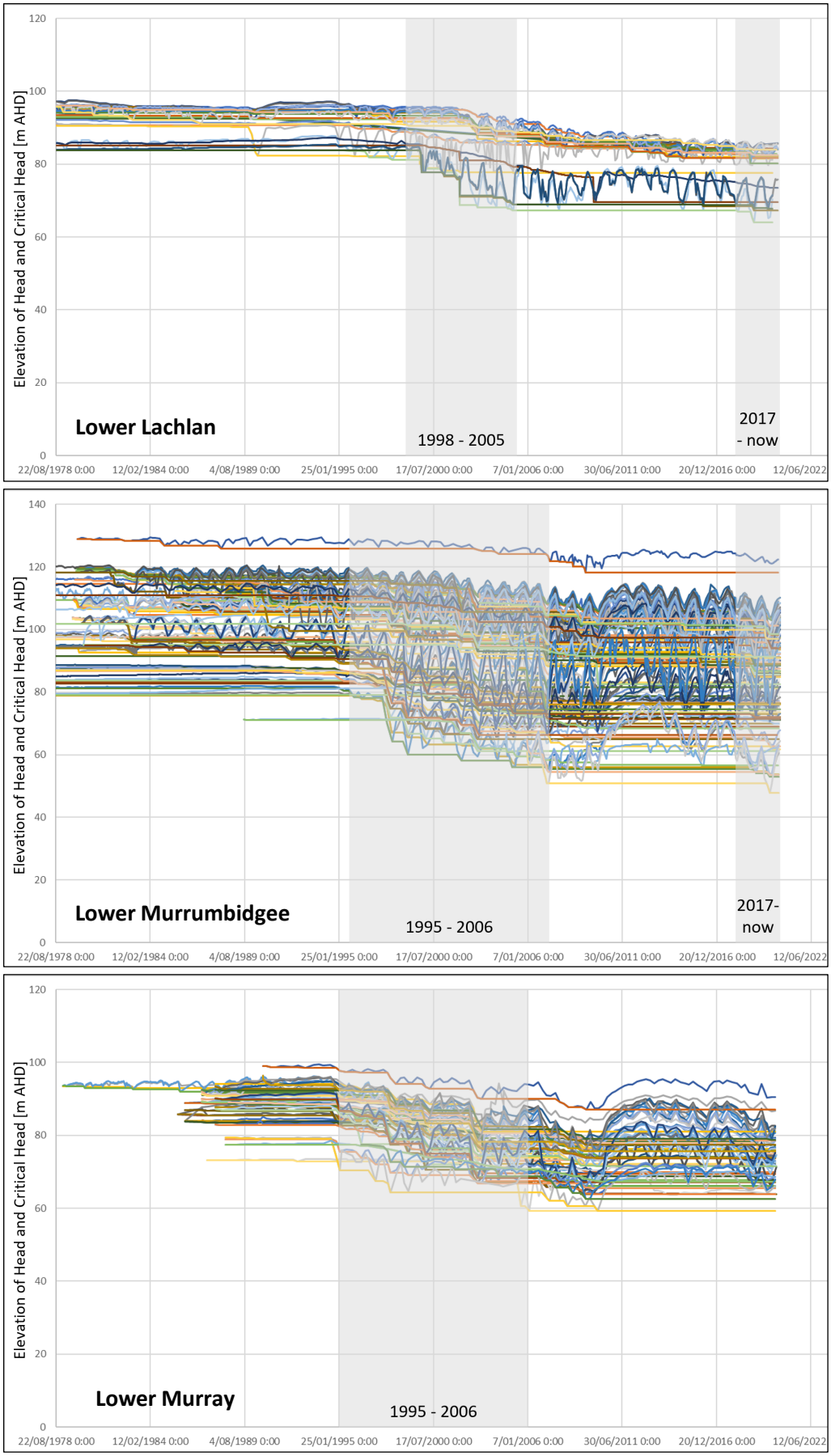

Figure 11 Groundwater levels and critical heads (CH) in the LL, LMB, and LM aquifers (for piezometers with a CH drop of more than 10 m over the entire record).

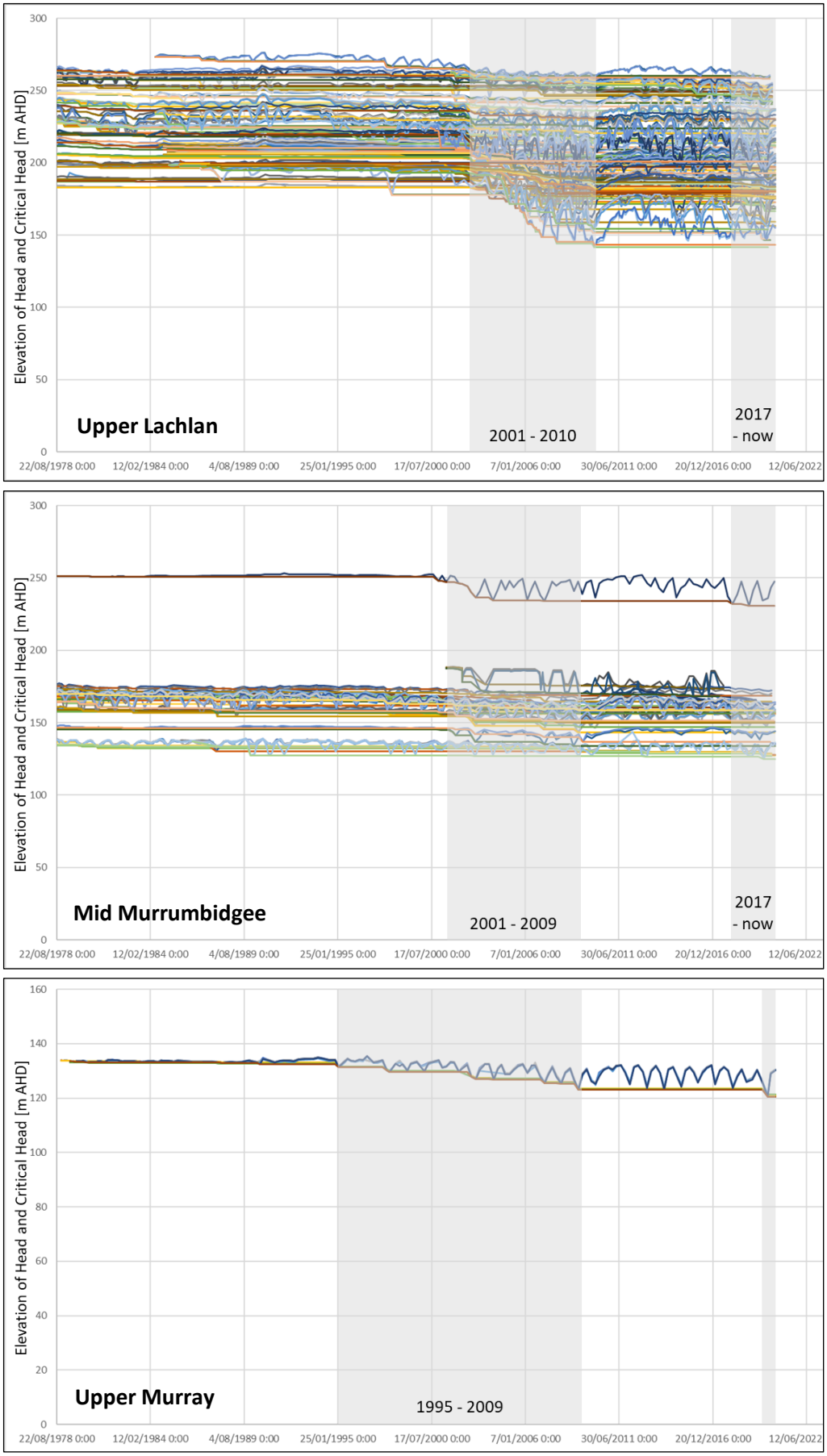

Figure 12 Groundwater levels and critical heads (CH) in the UL, MMB, and UM aquifers (for piezometers with a CH drop of more than 10 m over the entire record).

A less categorical and more numerical approach is to group piezometers into 'hypothetic layers' by intervals screen bottom depths based on their frequency distribution (Figure 13) with a bin of 50 m.

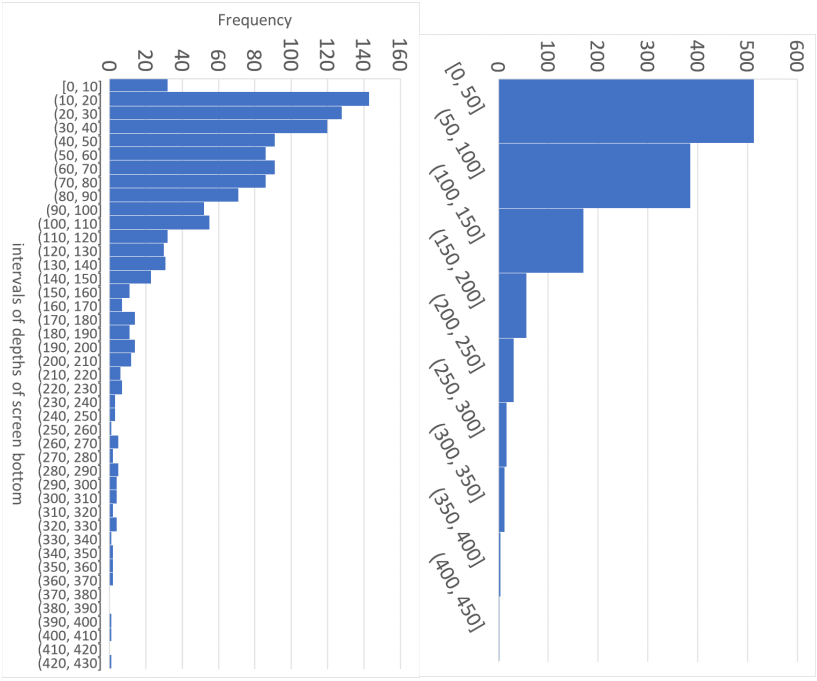

Figure 13 Frequency distribution of depths of screen bottoms of all 1196 piezometers.

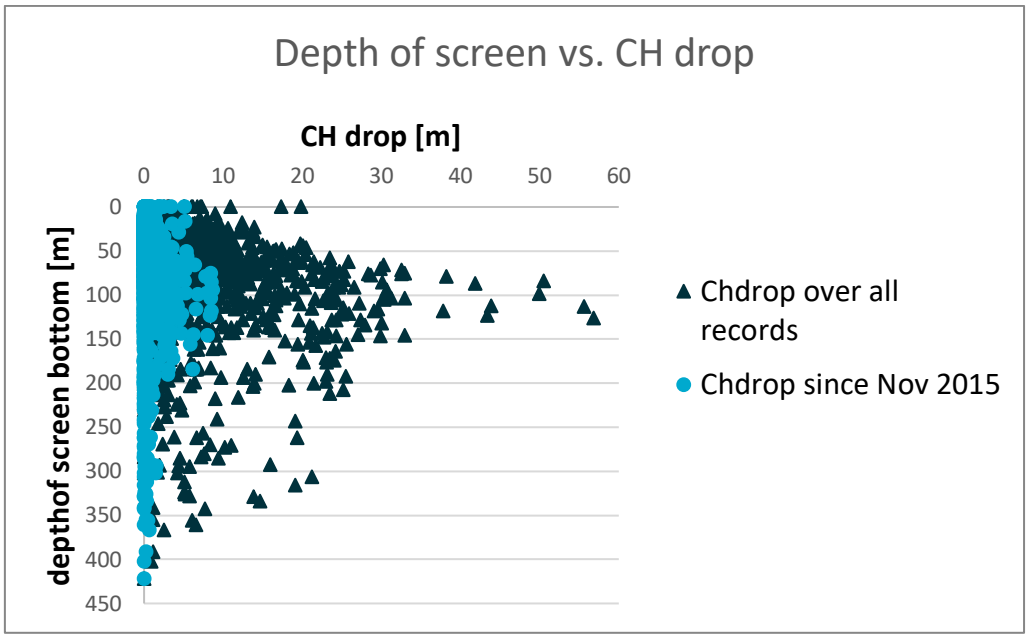

Figure 14 Relationship between depths of screen bottoms and critical head drop for the entire period of record keeping and over the InSAR observation period.

The horizonal and vertical distribution of critical head drop is illustrated for intervals of screen bottom depths and for aquifer layers the entire period of record keeping (Figure 15, Figure 16) and over the InSAR observation period (Figure 17, Figure 18).

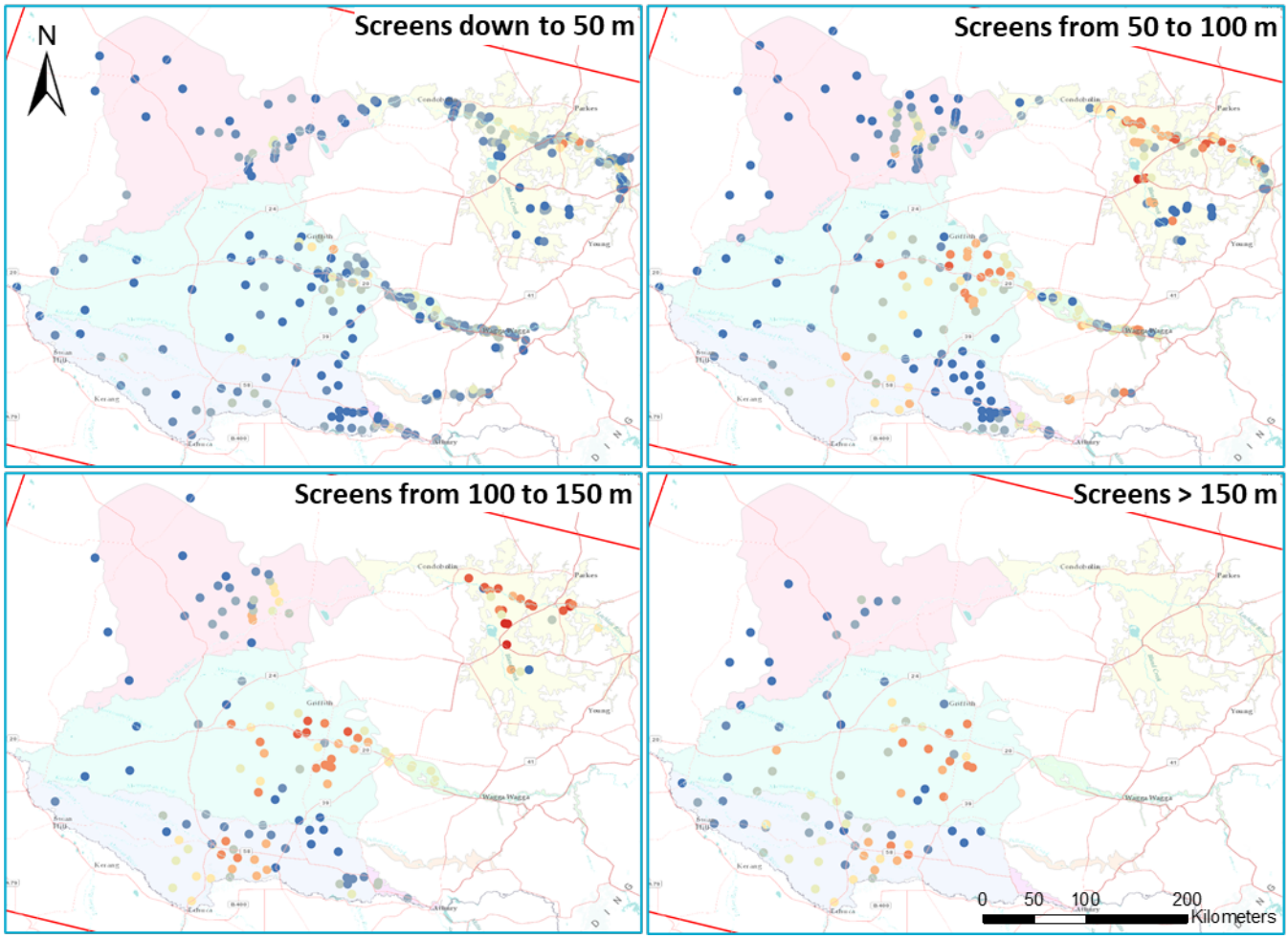

Legend

Critial Head drop since recording

- 0.000000 - 1.140000
- 1.140001 - 2.920000
- 2.920001 - 4.890000
- 4.890001 - 7.220000
- 7.220001 - 10.380000
- 10.380001 - 14.330000
- 14.330001 - 19.880000
- 19.880001 - 26.560000
- 26.560001 - 38.150000
- 38.150001 - 56.790000
- Area of Interest

Aquifers

- Bilabong Creek
- Lower Lachlan
- Lower Murray
- Lower Murrumbidgee
- Mid Murrumbidgee
- Upper Lachlan
- Upper Murray

Figure 15 Horizontal and vertical distribution (by intervals of screen bottom depths) of critical head drop since recording started.

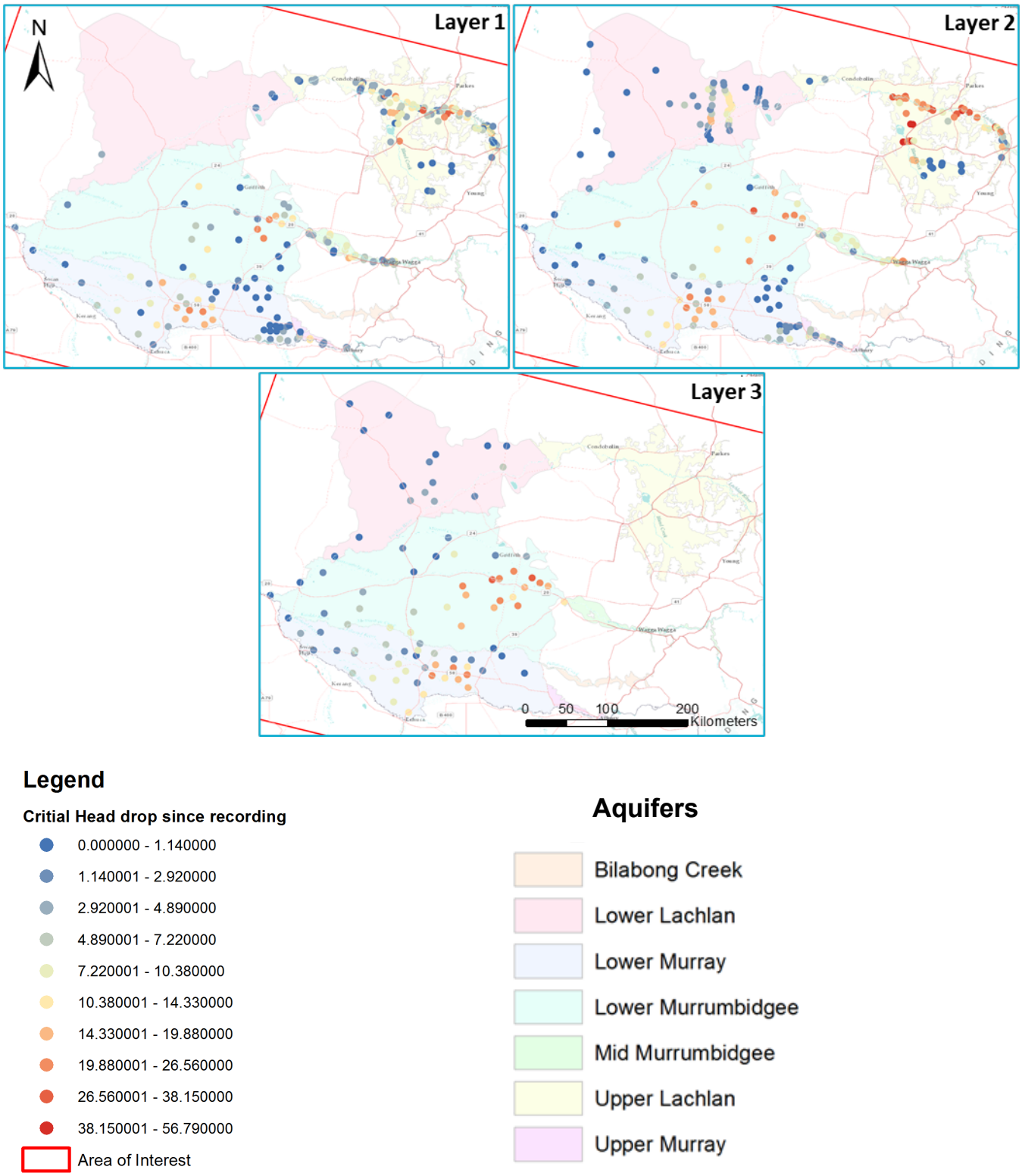

Figure 16 Horizontal and vertical distribution (by aquifer layers) of critical head drop since recording started.

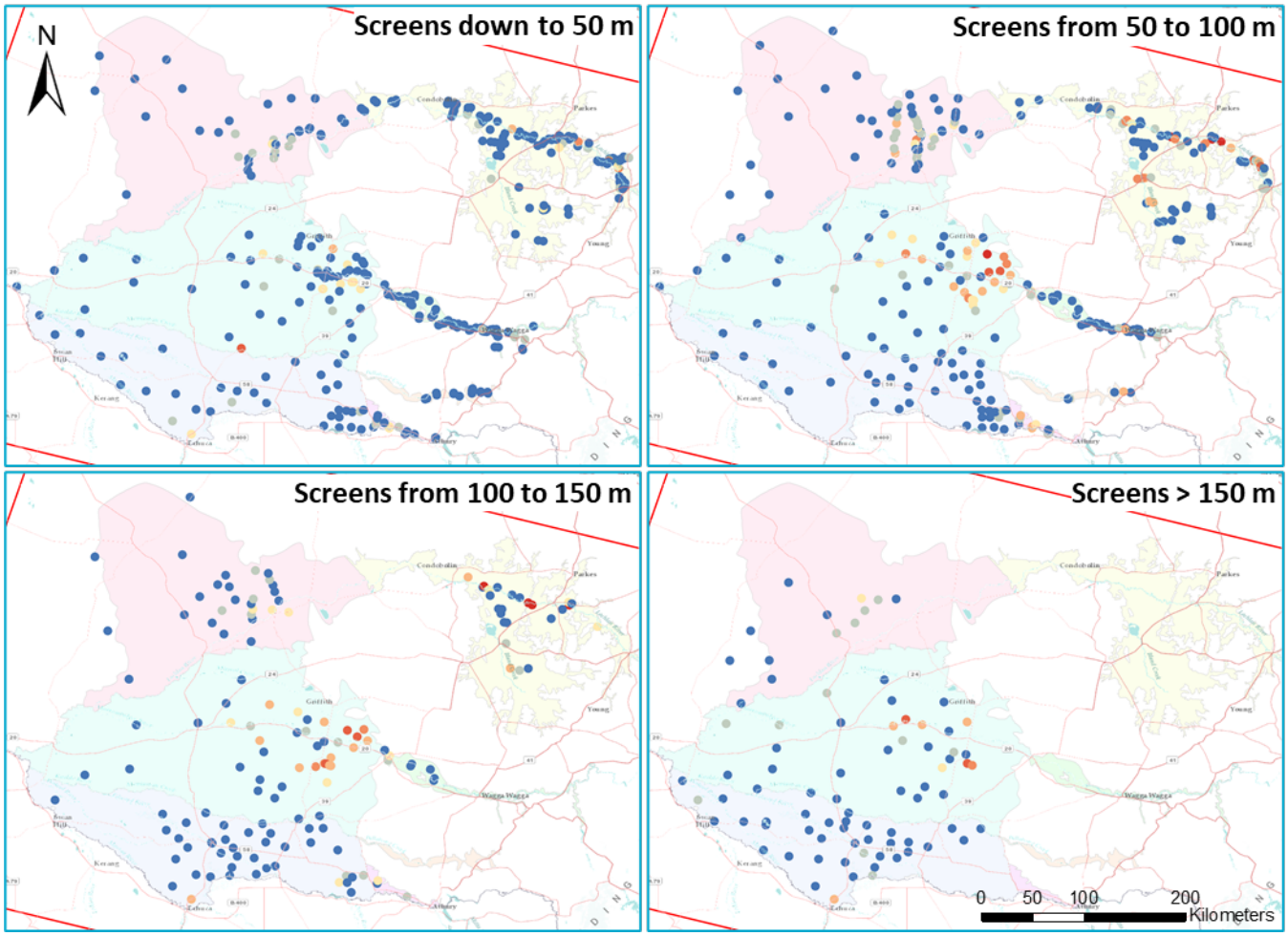

Legend

Critical Head drop since Nov 2015

- 0.000000 - 0.150000
- 0.150001 - 0.440000
- 0.440001 - 0.760000
- 0.760001 - 1.210000
- 1.210001 - 1.810000
- 1.810001 - 2.570000
- 2.570001 - 3.550000
- 3.550001 - 4.710000
- 4.710001 - 6.570000
- 6.570001 - 8.680000
- Area of Interest

Aquifers

- Bilabong Creek
- Lower Lachlan
- Lower Murray
- Lower Murrumbidgee
- Mid Murrumbidgee
- Upper Lachlan
- Upper Murray

Figure 17 Horizontal and vertical distribution (by intervals of screen bottom depths) of critical head drop since November 2015 (InSAR period).

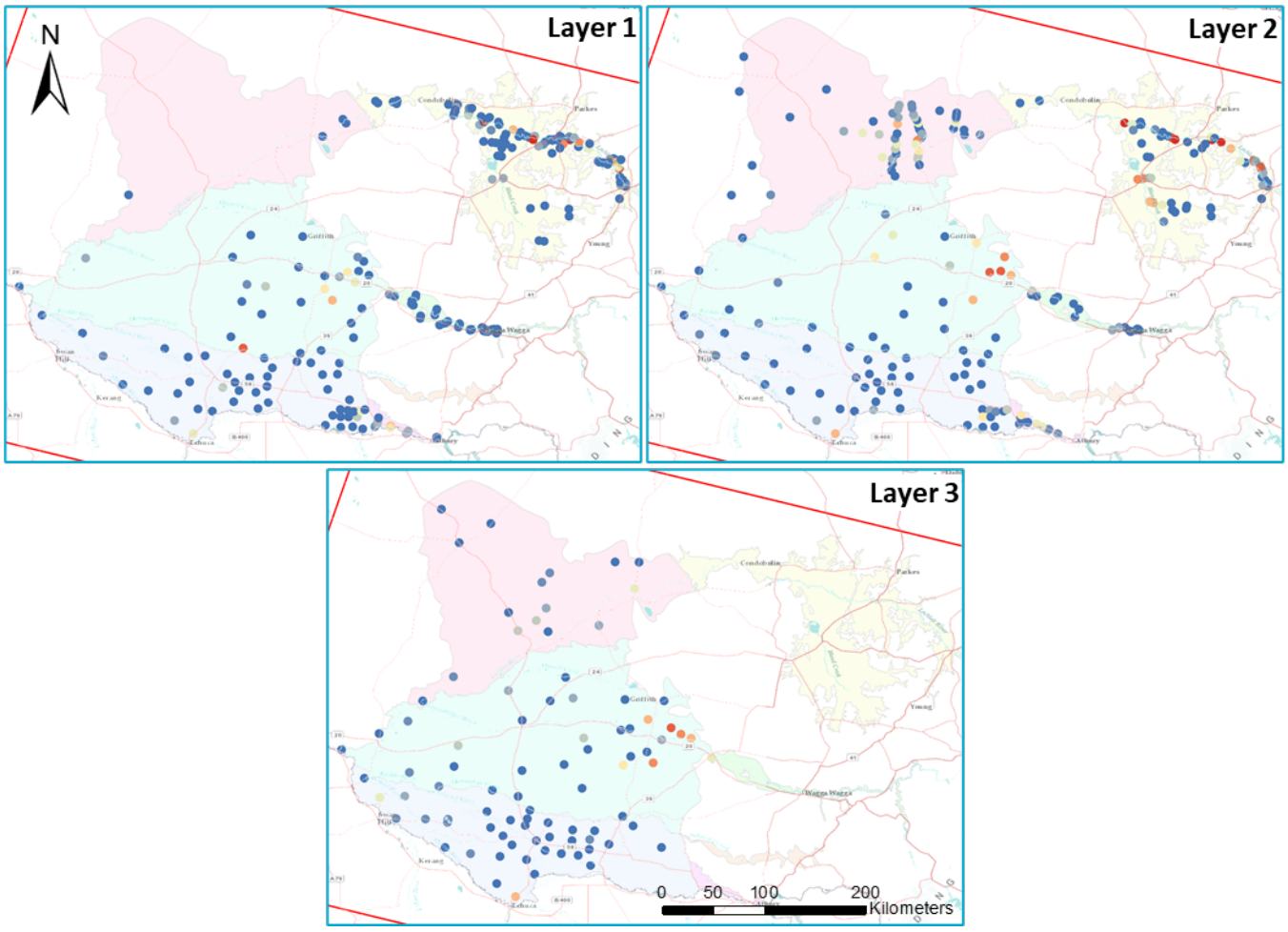

Figure 18 Horizontal and vertical distribution (by aquifer layers) of critical head drop since November 2015 (InSAR period).

Deepest drops of critical head for both the entire period of record keeping (Figure 14; Figure 15; Figure 16), occur in piezometers located horizontally in distinct clusters of the eastern LMB mostly in the area around Darlington Point, UL, and central LM. While the deepest critical head drops for the eastern LMB and UL concentrate in screen bottom intervals mainly in 50-100 m and 100-150 m, they dominate the central LM in deeper intervals (100-150 m and >150 m). The clustering of deep critical head drops by certain screen bottom intervals cannot be replicated by distinct layers. In the areas mentioned, deep critical head drops range across all three layers.

For the short InSAR observation period since November 2015 (Figure 14; Figure 17; Figure 18) only the UL and eastern LMB show significant critical head drop for the same screen bottom intervals mentioned above (50-100 m and 100-150 m). The central part of the LM does not exhibit any significant critical head drop for InSAR observation period. Piezometers screened at shallow depths down to 50 m and deep piezometers screened at depths > 150 m show little to no critical head drop. Deep critical head drops over this period seem to concentrate in Layer 2 for the eastern LMB and the UL, and in Layer 3 only for the eastern LMB

The primary expectation and hypothesis are (even prior to the actual InSAR vs. head correlation) that the presence or lack of critical head drop (and related dewatering from potentially present fine-grained interbeds/aquitards) will be reflected in the according presence or absence of inelastic subsidence. However, whether the presence of inelastic subsidence actually translates into InSAR deformation depends on whether the InSAR deformation signal is also clouded by noise from other factors, such as elastic expansion/compaction caused by groundwater head oscillations above critical heads, clay swelling/shrinking, and other surface factors.

Another expectation would to be to falsely assume that heavy groundwater usage always drives a drop in critical head. The maximum groundwater usage in the study in the InSAR observation period occurred in 2018-19 (Figure 19). However, in some areas, heavy groundwater usage is not followed by significant critical head drop as a result of previously deeper critical head drop and earlier preconsolidation (e.g., Hillston area in the eastern LL and some production bores along the LM). In addition, river or diffuse recharge my counteract drawdown.

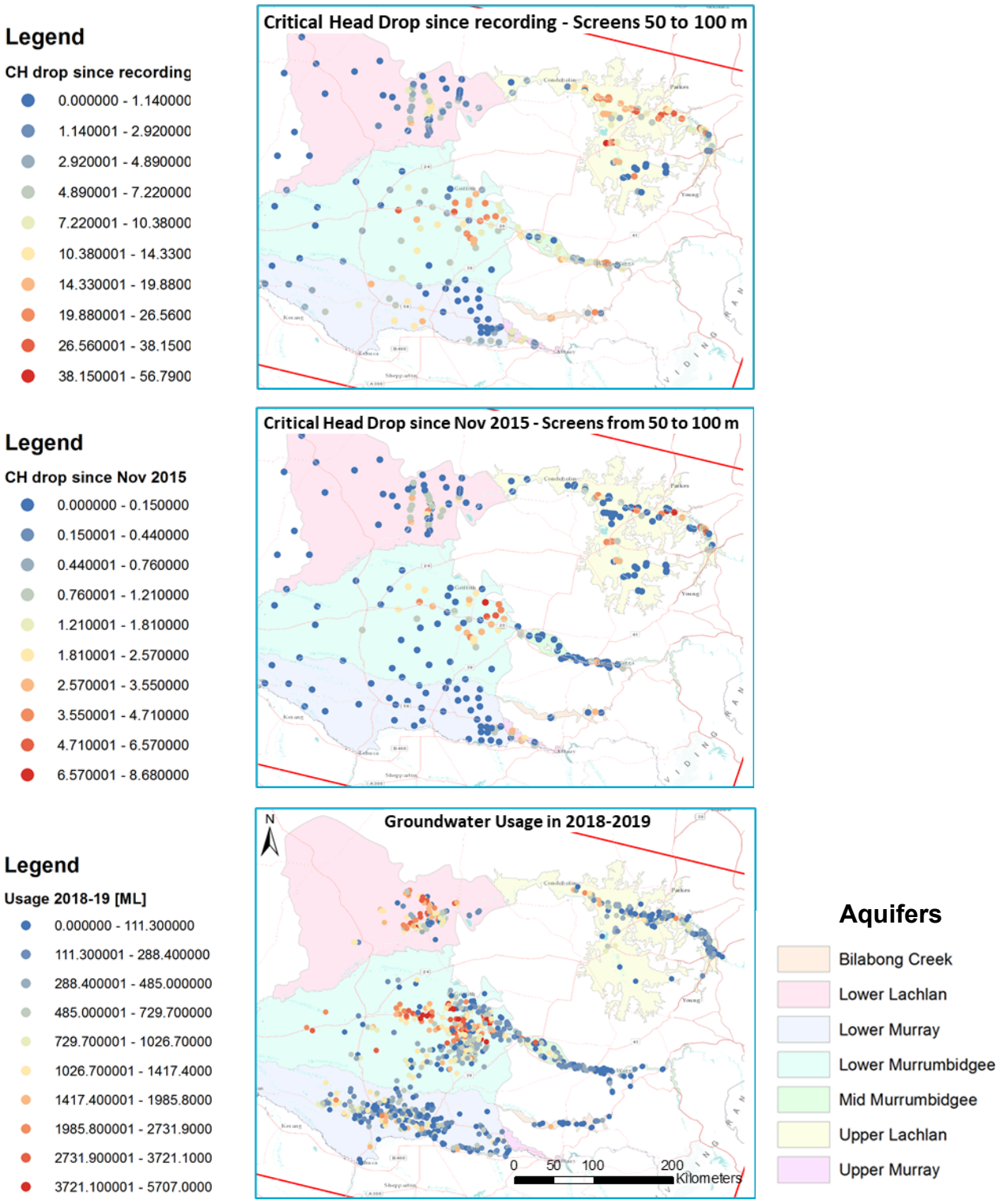

Figure 19 Comparison between Groundwater Usage in 2018-2019 (bottom) and Critical Head drop during InSAR period (middle) and since recording began (top) for a medium screen depth.

5.2 Temporal correlation between groundwater and ground deformation

The aim of this analysis is to determine whether InSAR deformation might be driven by inelastic compaction or rather elastic aquifer compaction and expansion as a result of critical head drop or head fluctuations above previous pre-consolidation heads, respectively.

Instead of focussing on the critical heads of select piezometers with deepest drawdowns which one would expect to drive subsidence (Castellazzi and Schmid, 2020), in this analysis we took an unbiased approach of including hydrographs of all bores. For hydrographs to be compatible with InSAR time series, the head and critical head time series were resampled based on the time stepping of the InSAR analysis for the period from November 2015 to May 2020. To upscale fine-scale InSAR displacement to the wider vicinity around the monitoring bore, a 15-by-15 pixel averaging kernel around each bore was used. Head and critical head time series were only considered if the number of measurements within the InSAR period exceeded a minimum of 10 and if at least 75% of the InSAR period was covered by measurements. Critical head time series were only used if groundwater level data exist prior to 2009 (6.7 years prior to the beginning of the InSAR era), assuring that any preconsolidation which potentially could have occurred during the Millennium Drought is accounted for.

As a first step, InSAR time series were compared with critical head (CH) and groundwater level (GWL) time series, once resampled based on InSAR time stepping. Scatter plots of all InSAR versus of all CH or GWL data pairs were created. Piezometers (or clusters of piezometers) that show a positive correlation between dropping critical heads and negative displacement from InSAR potentially indicate inelastic subsidence. A positive correlation between head fluctuations and InSAR displacement could point to elastic compaction or expansion.

As a second step, the data pairs of trends of InSAR displacement over the InSAR period are plotted against CH or GWL trends for each piezometer and clustered one time by aquifer and another time by temporal correlation coefficients. This allows to spot check whether aquifers are dominated by piezometers with wither good or poor correlations.

Critical head drop and InSAR time series

Figure 20 shows the histogram of correlation coefficients between InSAR and critical head drop time series of 416 piezometers. Overall, it is skewed towards a positive relationship between InSAR and critical head drop, implying that CH is an important factor for the InSAR displacement. However, CH drop can, by definition, only explain a negative, but not positive (ground uplift) InSAR displacement.

The following discusses firstly examples of strong positive correlations between InSAR and CH time series, of less strong and less meaningful correlations when the number of critical head drops declines, and finally of not physically meaningful negative correlations between dropping CH, but positive InSAR displacement.

Figure 21 shows two examples of strong and positive correlation between InSAR and CH time series (R = 0.66; 0.8), which supports our hypothesis that, for some piezometers, CH is an important factor for ground displacement. Figure 22 shows another example of positive, strong temporal correlation between InSAR and CH, but this time for three piezometers of the same bore

(GW030406) screened to different depths (R = 0.83; 0.78; 0.78). However, for the deeper piezometers, the number of CH drops within the InSAR period declines down to two or even just one drop. Since InSAR displacement in this case is invariant over most of the time with critical head, the correlation strength may be overestimated. Another way of representing the linear correlation would be to correlate the means or medians of InSAR displacement over periods of constant CH. However, using the median may better reflect the causal relationship between the two variables: Consolidation follows dewatering after some delay, which would not lead to a normal, but rather skewed, distribution of InSAR displacement over periods of constant CH. Finally, Figure 23 demonstrates two cases of an unrealistic negative correlation between InSAR and CH, i.e., a decline of CH with a positive InSAR displacement. It implies that surface factors rather than groundwater dynamics could affect InSAR displacement.

Figure 24 shows for all analysed piezometers the relationship between InSAR trends and CH trends in different aquifers (A) and how strong the temporal correlation is (B). The piezometers in the UL generally show a combination of larger CH decreasing trend as well as a larger declining InSAR trend. This can be observed for the LL and the UM as well, although the magnitude of the CH trend is smaller with a few exceptions. In contrast, the LMB features an equal distribution of positive and negative InSAR trends. Piezometers with strong positive correlations between InSAR and CH drop time series can generally be found for combinations of large negative trends of both CH drop and InSAR displacement. Those strongly positive-correlating piezometers mostly fall into the UL, LL, and LMB aquifers, which is not surprising for the UL and LL as most piezometers there exhibit a combination of dropping CH and negative InSAR displacement. However, for the LMB, it seems that an equal number of piezometers show moderately to strong positive as well as negative correlations. The latter is most likely due surface factors related to land use, soil, and the influence of climate and the Murrumbidgee river.

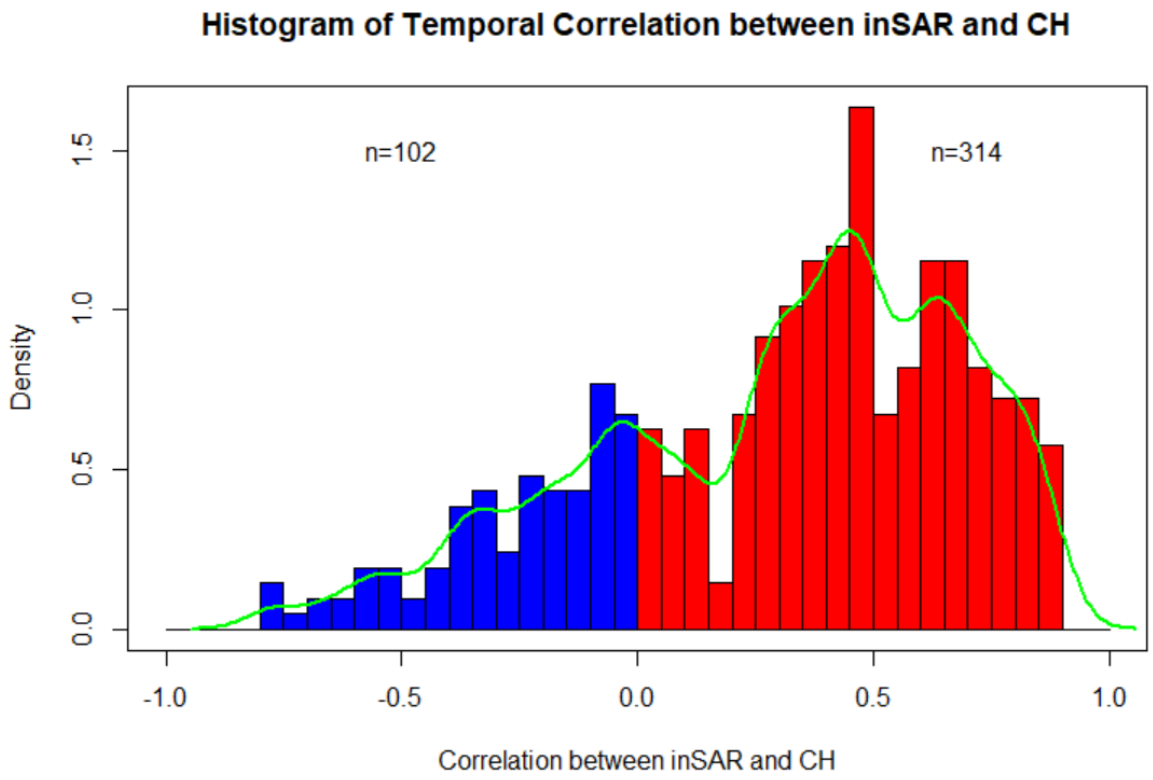

Figure 20 Histogram of temporal correlation between InSAR and CH.

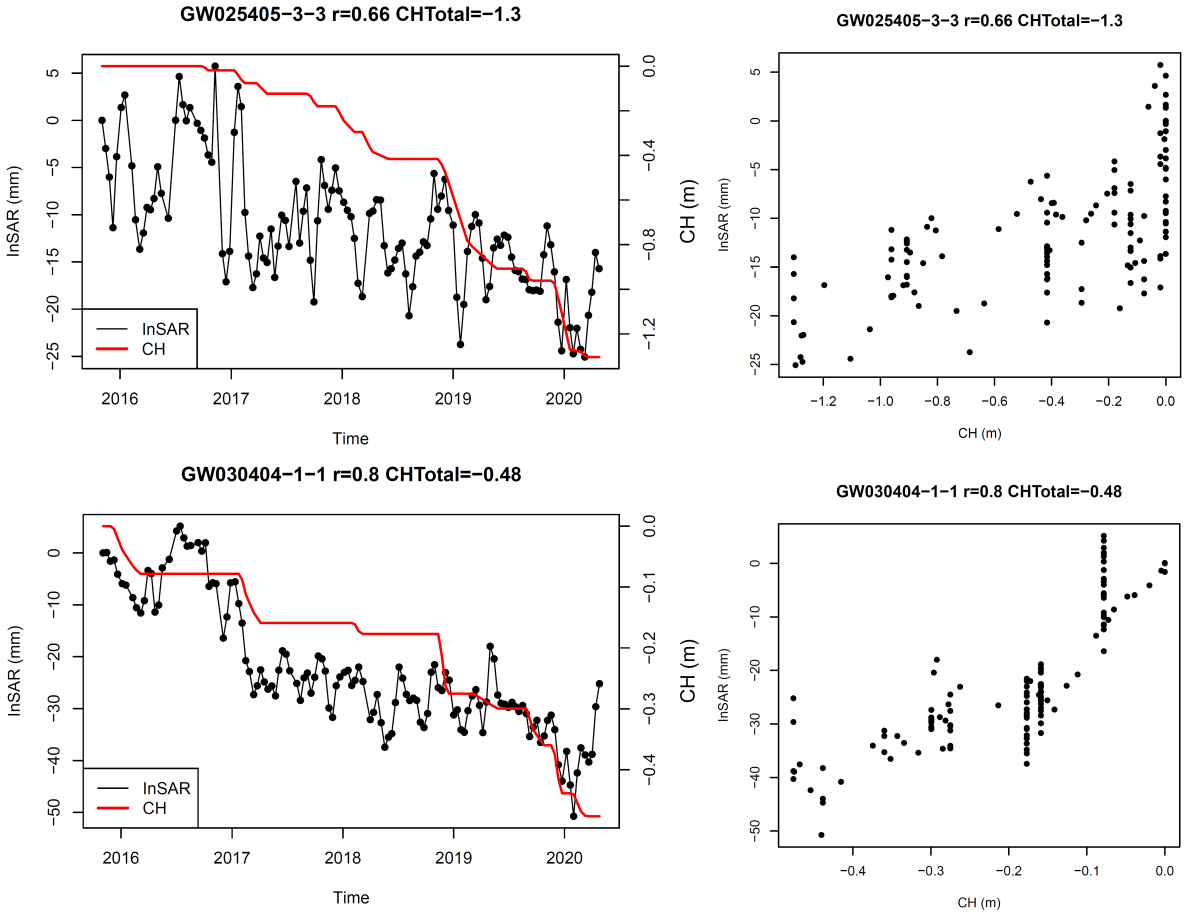

Figure 21 Two examples of strong and positive correlations between InSAR and CH.

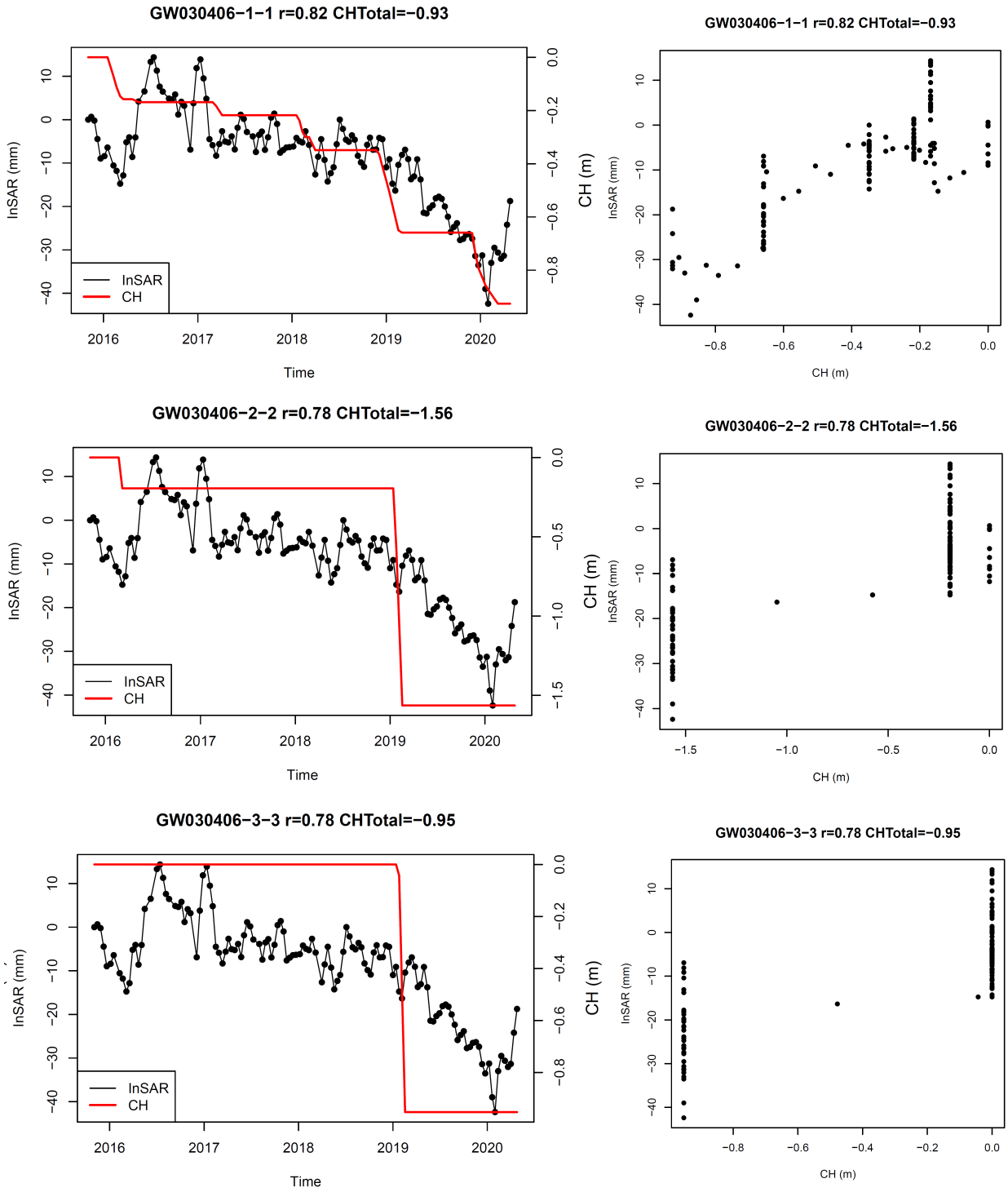

Figure 22 Example of InSAR and CH at same bore with different piezometers.

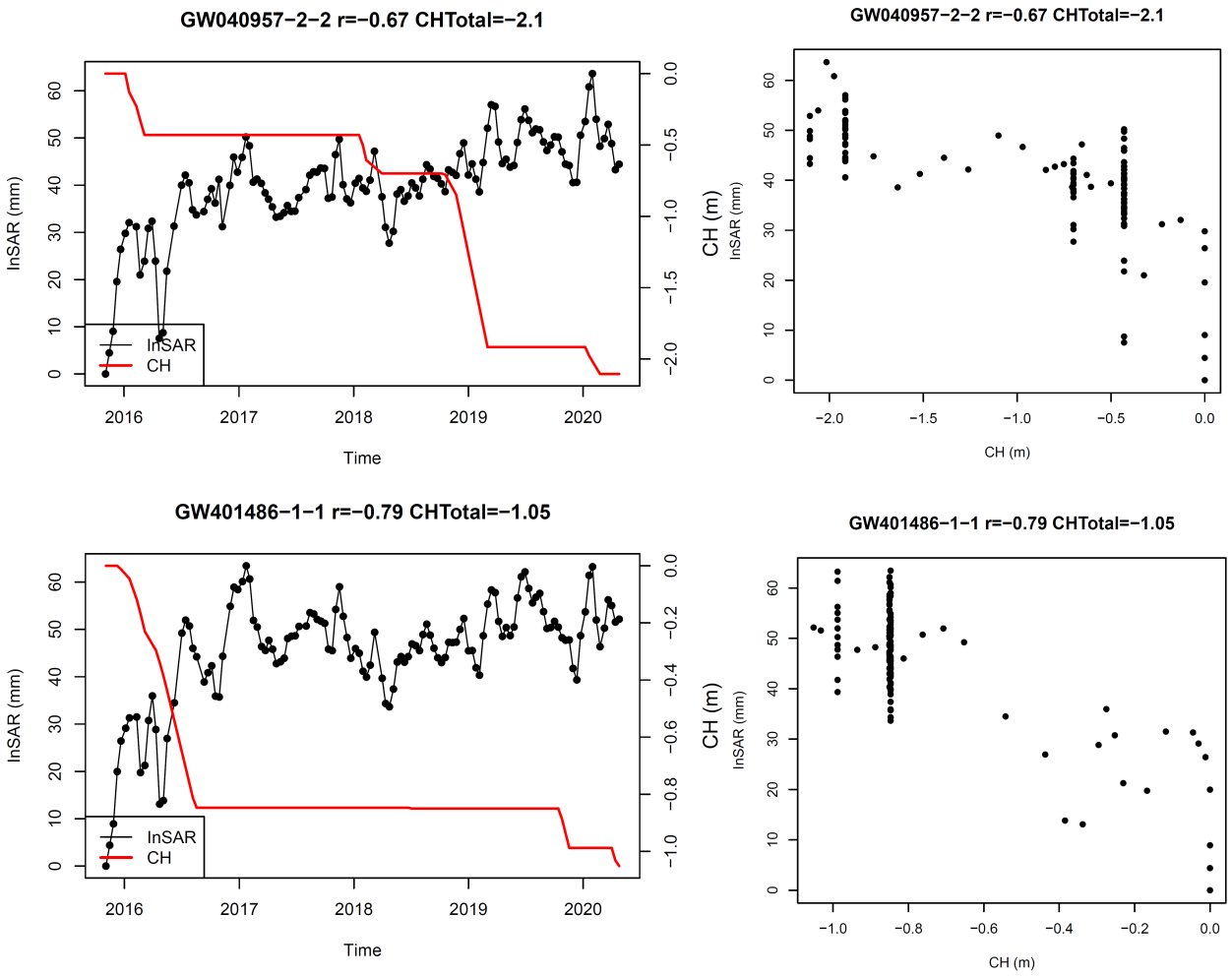

Figure 23 Examples of negative correlation between InSAR displacement and CH.

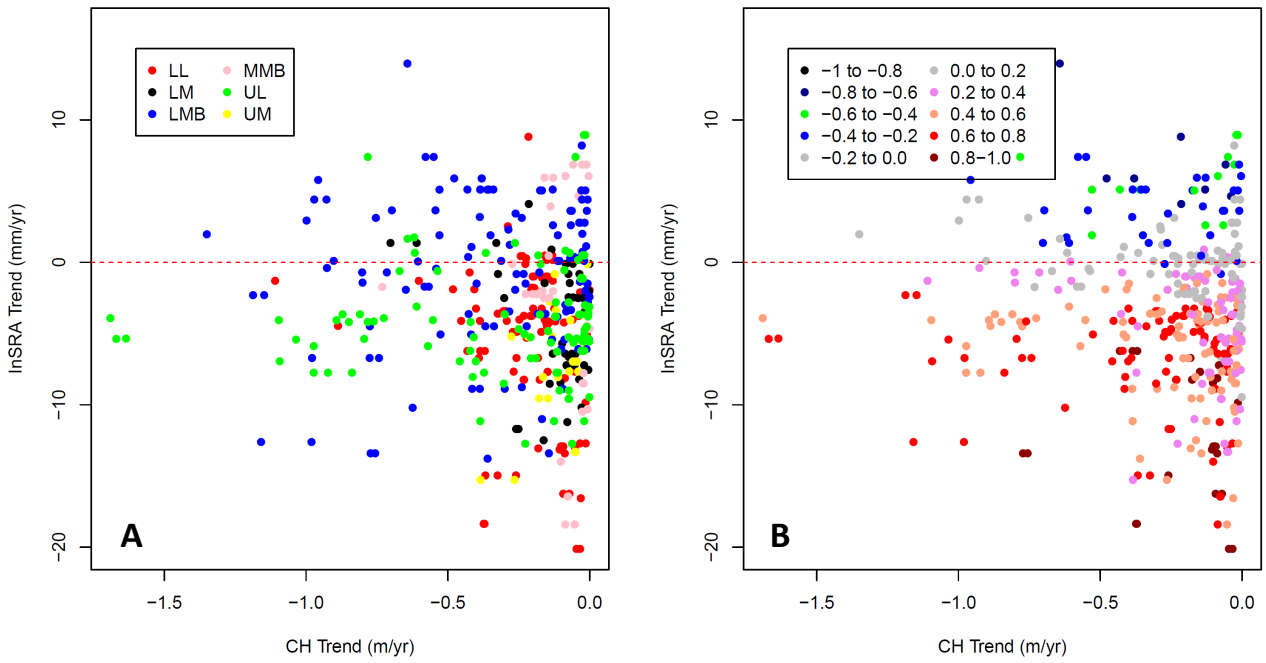

Figure 24 Correlation between InSAR and CH trends by aquifer (A) and by correlation coefficient (B).

Groundwater level and InSAR time series

Figure 25 shows the histogram of correlation coefficients between InSAR displacement and groundwater level (GWL thereafter) in 975 sites. Overall, is it skewed towards a positive relationship between InSAR and GWL time series in the last 5 years. However, 237 piezometers still show a negative correlation between InSAR and groundwater level. It suggests that other surface factors could have an impact on positive InSAR displacement while GWL is trending downward.

The following discusses firstly examples of strong positive correlations between InSAR and GWL time series and the expected and some unexpected impacts of seasonality in deeper piezometers. In addition, similarly to Figure 23, we also present examples of negative correlations between dropping GWL, but positive InSAR displacement.

Figure 26 shows two examples of strong, positive correlations between InSAR displacement and GWL (R = 0.93; 0.93). Both InSAR displacement and GWL show decreasing trends in the last 5 years implying that the InSAR deformation is driven by elastic aquifer compaction and expansion. Figure 27 and Figure 28 show two examples of moderately positive correlations between InSAR displacement and GWL trends for different piezometers of the same bore screened to different depths (GW036366 with R = 0.64; 0.64; 0.63 and GW030258 with R = 0.73; 0.72; 0.71). GW036366 (Figure 27) shows a stronger seasonal variability for shallower then for deeper piezometers, which is expected because the shallow piezometer generally responds stronger to seasonal change of hydroclimate conditions, such as rainfall, PET, groundwater recharge. In contrast and unexpectedly, GW030258 (Figure 28) shows that the deeper piezometer has a larger seasonality than a shallower one. This opposite pattern of seasonality of groundwater levels indicates that other important factors may affect groundwater dynamics, which warrants further investigation. Finally, Figure 29 shows two piezometers with an unrealistic and negative correlation between positive InSAR displacement and declining GWL trends. They also do not echo each other. Again, it indicates that surface factors rather than groundwater dynamics could affect InSAR displacement.

Figure 30 shows for all analysed piezometers the relationship between InSAR trends and GWL trends in different aquifers (A) and how strong the time series correlation is (B). The piezometers in the UL and LMB generally show a combination of larger negative GWL trends and larger declining InSAR trend. However, the LMB and the UL also show combinations of positive InSAR displacement trends and negative GWL trends. The GWL trend of piezometers in the LL and MMB generally is small or invariant with InSAR displacement trends. Generally strong positive time series correlations are found at piezometers with large negative GWL and InSAR displacement trends. This seems to indicate that GWL oscillations around an overall negative GWL trend may rather impact on elastic compaction than on expansion. Elastic expansion would require rising GWLs (above previously established critical heads) with positive correlations between at piezometers with both positive GWL trends and positive InSAR trends. However, instead, negative time series correlations are found at piezometers with mildly negative GWL trends and mildly positive InSAR displacement trends, meaning that groundwater is likely not related to this uplift.

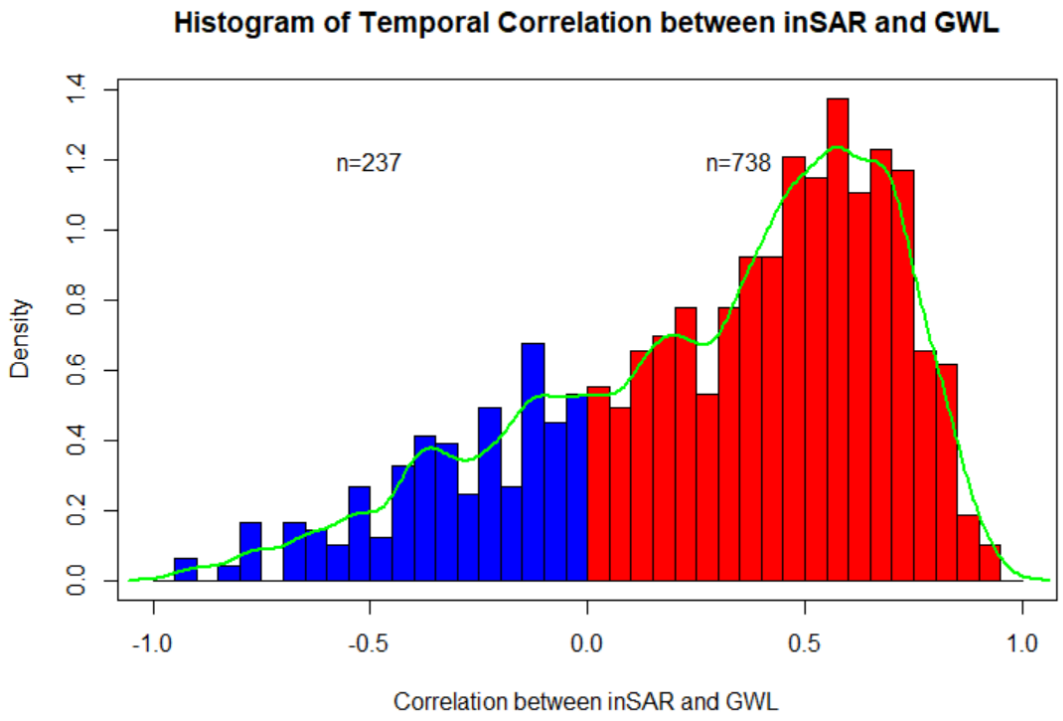

Figure 25 Histogram of temporal correlation between InSAR trend and groundwater level (GWL).

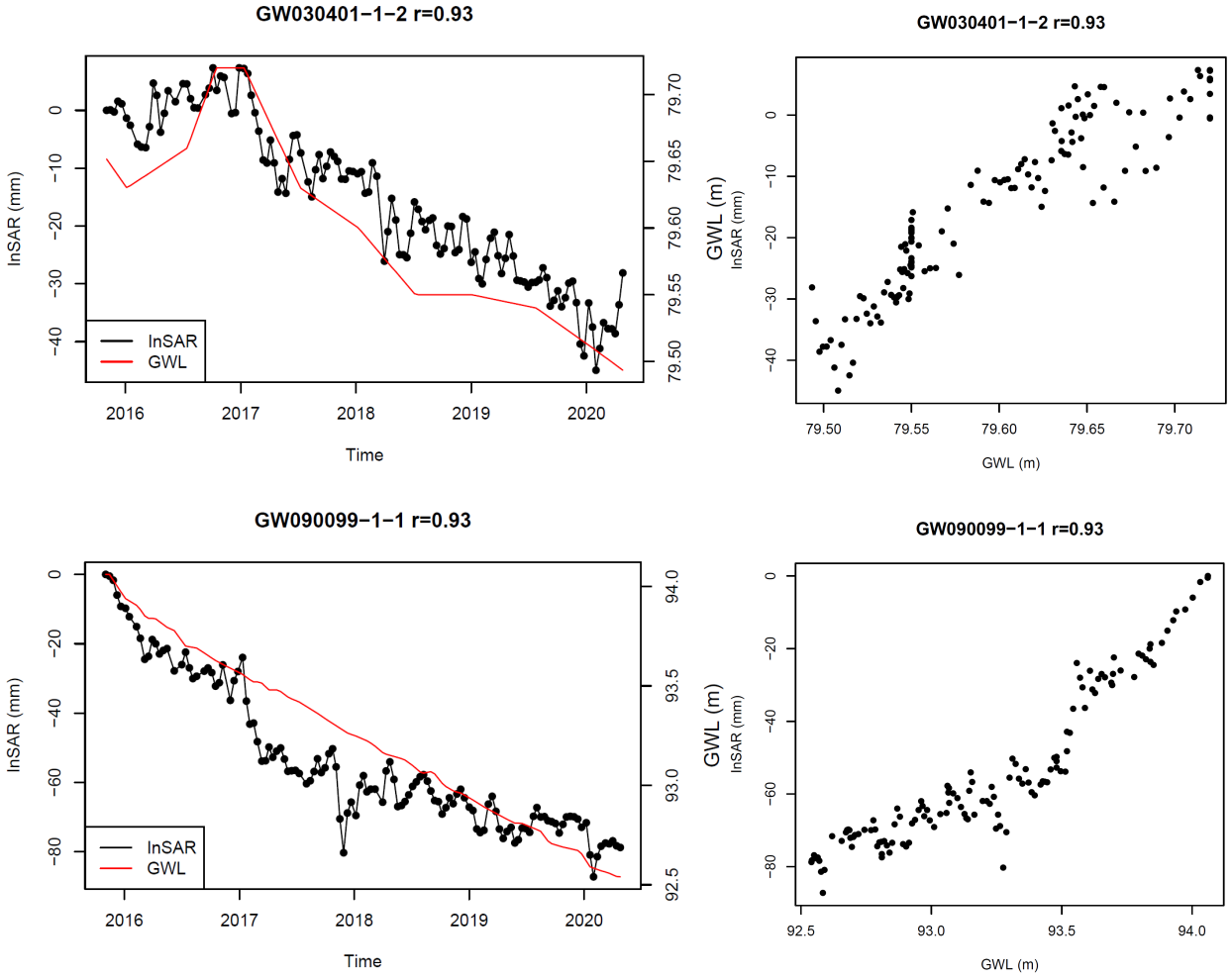

Figure 26 Examples of strong, positive correlation between InSAR displacement and GWL.

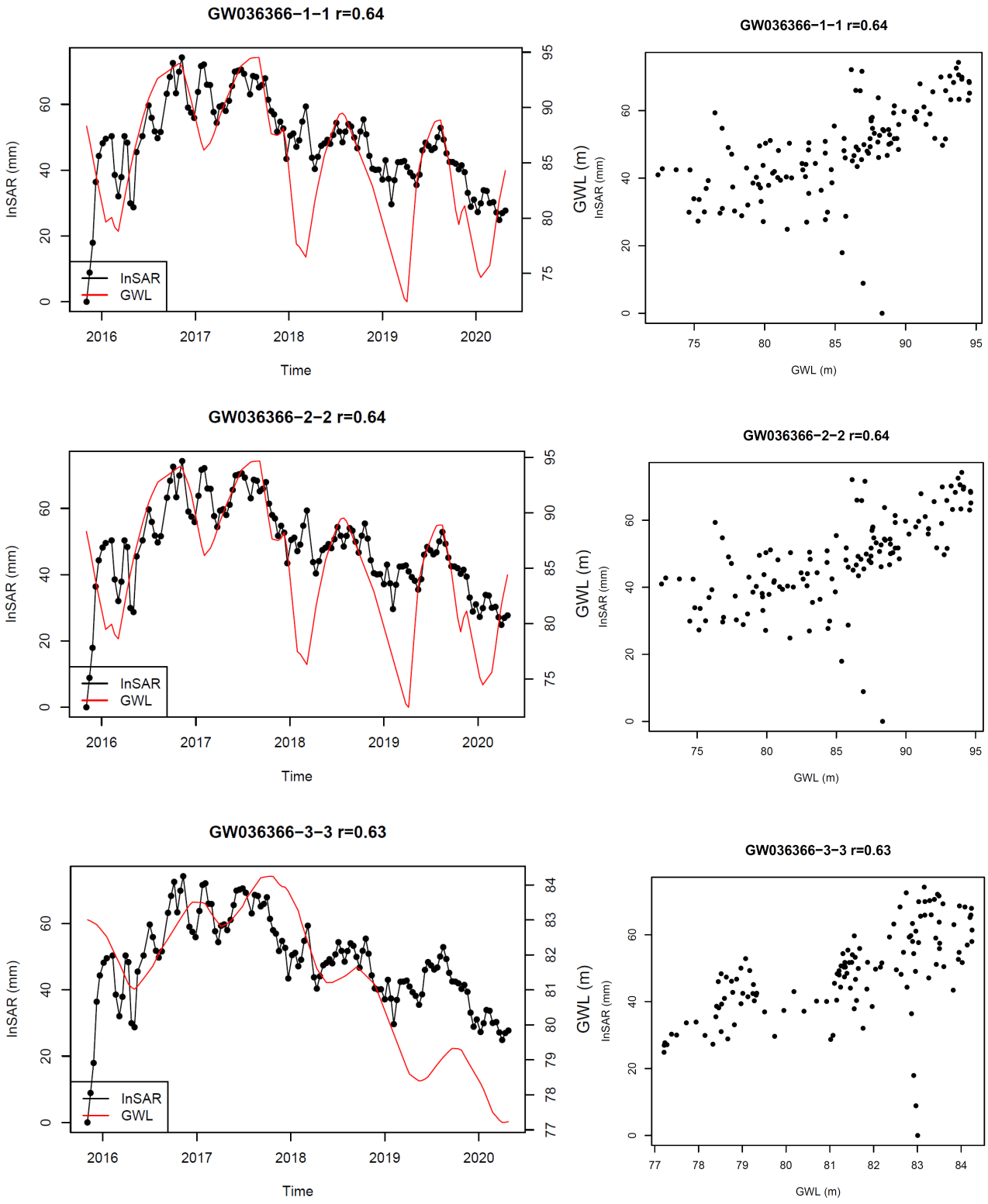

Figure 27 Example of correlation between InSAR displacement and GWL at bore GW036366 with 3 different piezometers.

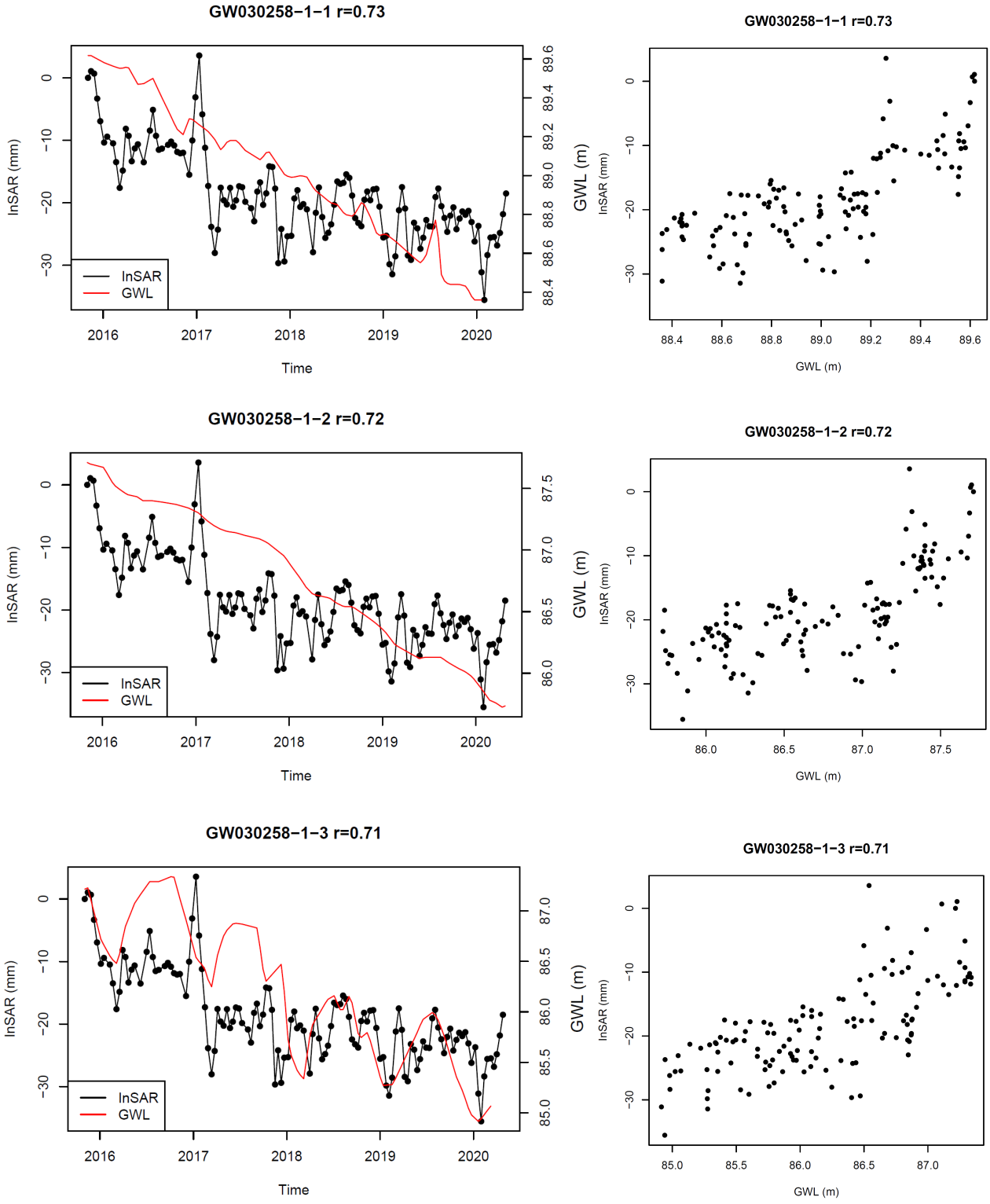

Figure 28 Example of correlation between InSAR displacement and GWL at bore GW030258 with 3 different piezometers.

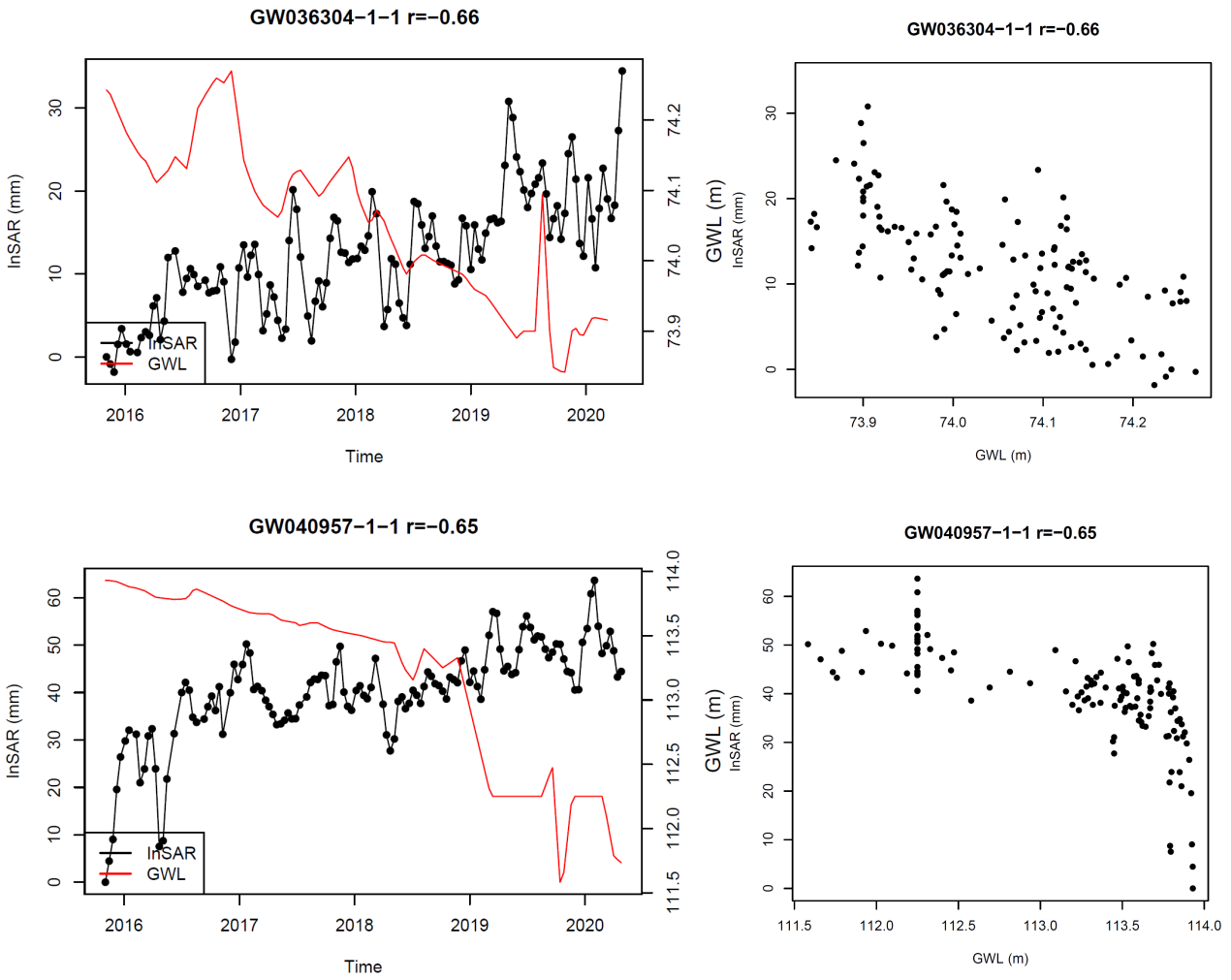

Figure 29 Examples of negative correlation between InSAR displacement and groundwater level.

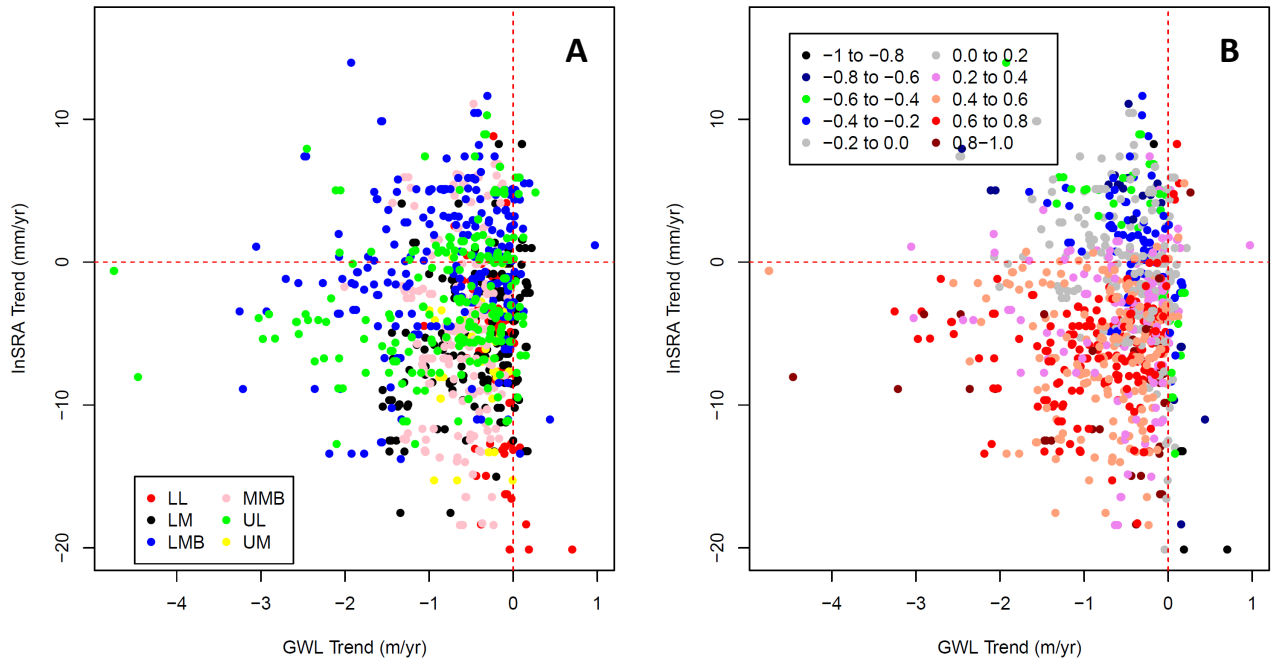

Figure 30 Correlation between InSAR and head trends by aquifer (A) and by correlation coefficient (B).

5.3 Spatial distribution of temporal correlations between groundwater and ground deformation

The spatial distribution of positive or negative correlations between InSAR displacement and critical head drop time series is displayed in Figure 31 (for vertical distribution by intervals of screen bottom depths) and Figure 32 (for vertical distribution by aquifer layers). The spatial distribution of correlations between InSAR displacement and groundwater head oscillation time series is displayed analogously in Figure 33 and Figure 34.

Positive correlations

Horizontal distribution

The horizontal distribution of strong positive correlations between critical head and InSAR displacement time series is concentrated in clusters around the eastern LL and to some extent the eastern LMB, and the river corridors of the UL and the UM. The MMB and most of the LM are nearly free of data points, as heads did not exceed historic minima established prior to the InSAR observation period.

In contrast, the horizontal distribution of strong positive correlations between head oscillations and InSAR displacement time series is much more widespread and denser than the distribution of piezometers with good CH-vs-InSAR-correlation (with clusters in the eastern LL, the river corridor of the UL, the eastern LMB, the MMB, the central LM, and the UM).

Vertical distribution

Both critical heads and head oscillations of piezometers of each area appear to correlate well with InSAR not across the entire alluvium, but only for certain layers (Table 5 and Table 6). The highest density of piezometers with good positive CH-vs-InSAR correlation in each area is marked in red.

Evidently, the aquifers in the lower parts of the Lachlan, Murrumbidgee and Murray catchments experience most of the good positive correlation between InSAR displacement and both critical head (CH) or head hydrographs (suggestive of either inelastic compaction or elastic compaction/expansion) in medium to deep alluvium (50-150m; Layers 2 and 3 - Calvil/Lachlan and Renmark formations). In contrast, the aquifers to the east in the mid and upper parts of the catchments demonstrate the same in shallower depths (0-100m; Layers 1 and 2 - Cowra/Shepparton and Calvil/Lachlan formations).

The good correlation between CH and InSAR at those depths is not surprising as it was anticipated in Figure 17 and Figure 18 for the eastern LL , the eastern LMB, and the river corridor of the UL simply based on maximum critical head drops, which assumes that the dewatering and resulting consolidation are indeed the main drivers for InSAR deformation.

Negative correlations

Strong negative correlations, where a positive InSAR displacement indicates an uplift while critical head or groundwater levels drop instead are typical for the aquifers in the lower parts of the catchments, in areas where surface factors prevail (e.g., along Murrumbidgee and Murray Rivers).

However, there are also a number of areas afar from the rivers where such a negative correlation exists.

Non-groundwater surface factors near the rivers (e.g., recharge, flooding, surface-water irrigation, etc.) are likely to have an impact on surface deformation irrespective of the course of critical heads or head hydrographs. However, a causality for 'good' negative correlations cannot be inferred from this single-variable correlation analysis.

Table 5 Vertical distribution of piezometers with strong, positive correlation between CH and InSAR deformation (red: highest density of piezometers with strong, positive correlation in each area).

	Intervals of screen bottom depth [m below RL]				Aquifer Layers		
	0-50	50-100	100-150	>150	1	2	3
Eastern LL	x	x	x			x	x
Eastern LMB		x	x			x	x
Western LM	x			x			x
River corr. UL	x	x	x		x	x	
MMB							
UM	x	x	x		x	x	

Table 6 Vertical distribution of piezometers with strong, positive correlation between head and InSAR deformation (red: highest density of piezometers with strong, positive correlation in each area).

	Intervals of screen bottom depth [m below RL]				Aquifer Layers		
	0-50	50-100	100-150	>150	1	2	3
Eastern LL		x	x			x	x
Eastern LMB	x	x	x	x	x	x	x
Central LM		x	x	x	x	x	x
River corr. UL	x	x	x		x	x	
MMB	x	x			x	x	
UM	x	x	x		x	x	

5.4 Results

The temporal correlation analysis seems to indicate that isolated areas may be affected by inelastic subsidence corroborated by a strong correlation between the drop in CH and InSAR-derived compaction (eastern LL, some hotspots in the LMB (e.g., around Coleambally), along the river corridors of the UL and UM). This compaction appears to follow the dewatering of the medium to deep alluvial aquifer in the eastern LL and LMB that coincides with the Calvil/Lachlan and Renmark formation and of the shallow to medium deep aquifer in the UL and UM that is represented by the Cowra/Shepparton and Calvil/Lachlan formations). Elastic compaction and expansion evidenced by a strong positive correlation between head oscillations and InSAR deformation is more widespread in its horizontal distribution but focusses in each area on the same aquifer depths or layers as the CH-vs-InSAR-derived compaction.

All these findings need to be viewed in the context that the temporal correlation analyses between CH drop or head and InSAR displacement time series are single-variable and not multivariate correlation analysis. Even findings of strong correlations between CH drop or head and InSAR displacement need to be treated with caution as other influential parameters are ignored. However, when temporal correlations are week or negative, we can sufficiently infer that other non-groundwater, surface-related parameters are at play. The following section (section 6)

discusses a multi-factorial 'Random Forest' analysis between different variables and InSAR deformation, which may provide some answers as to which predictors (and where in space) have more or less impact on spatially distributed InSAR deformation trends over the 5-year observation period.

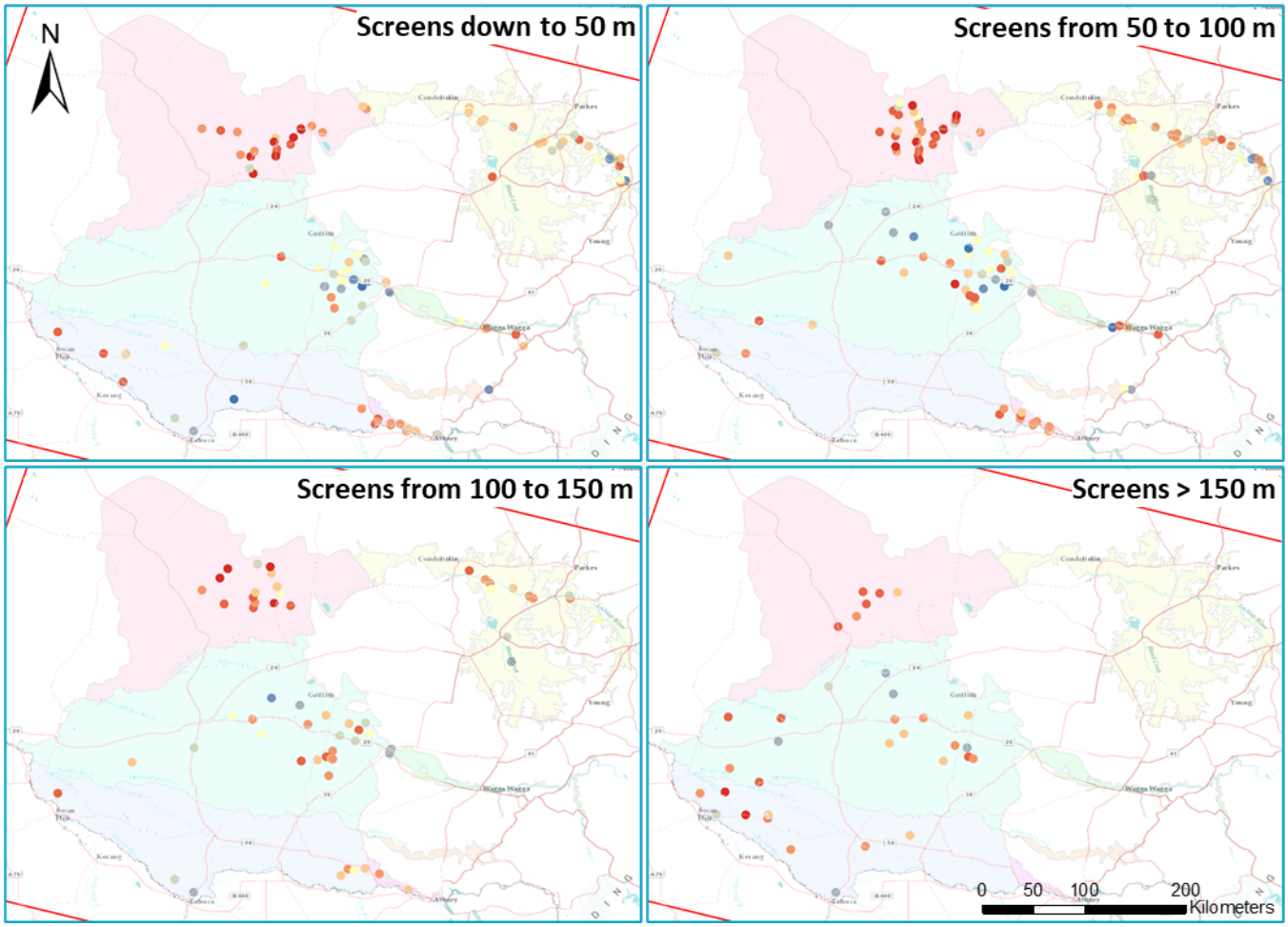

Figure 31 Horizontal and vertical distribution (by screen depths of bores) of positive and negative correlation between critical head drop and InSAR deformation time series.

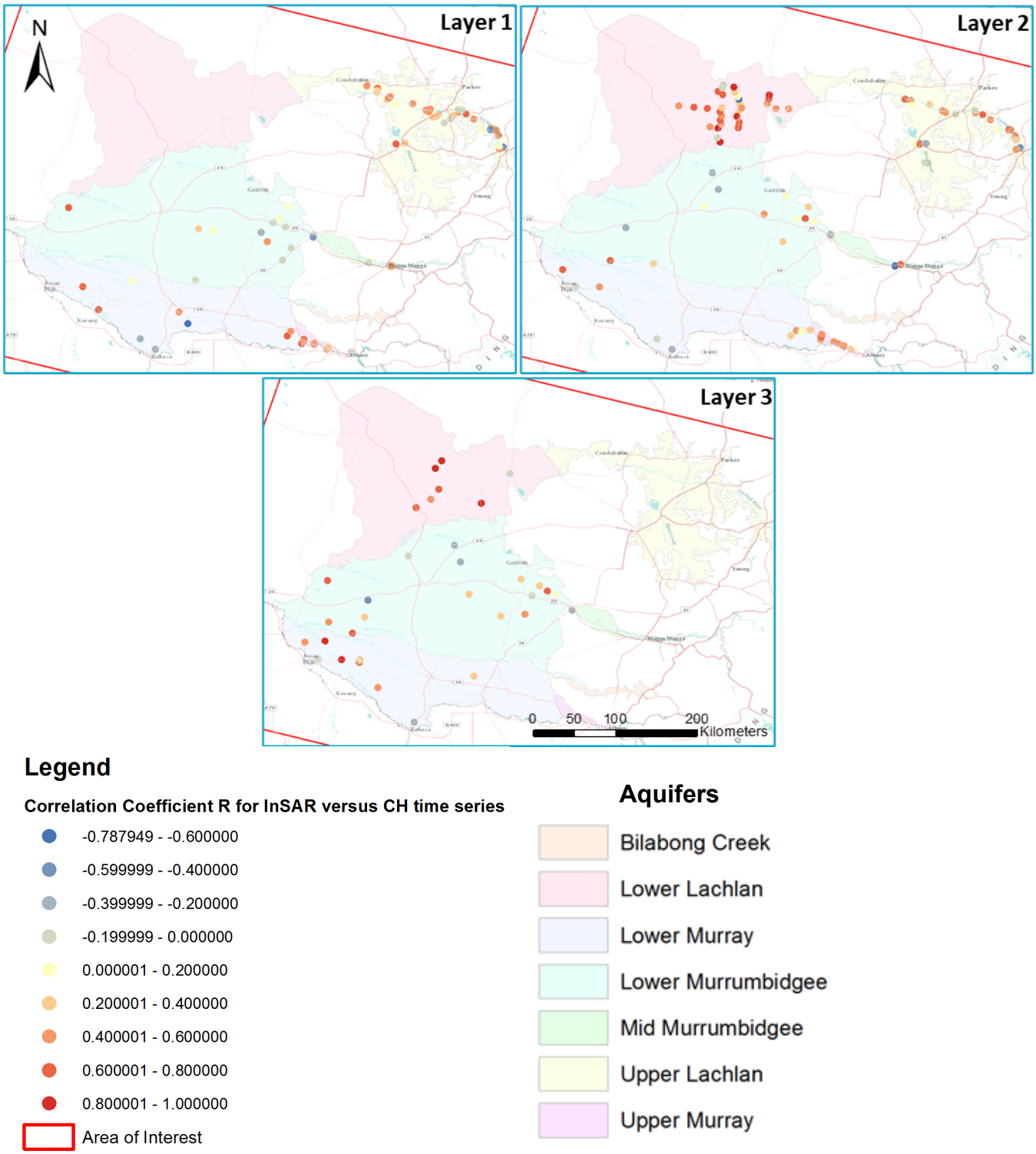

Figure 32 Horizontal and vertical distribution (by aquifer layers) of positive and negative correlation between critical head drop and InSAR deformation time series (layer attribution to bores derived from groundwater models).

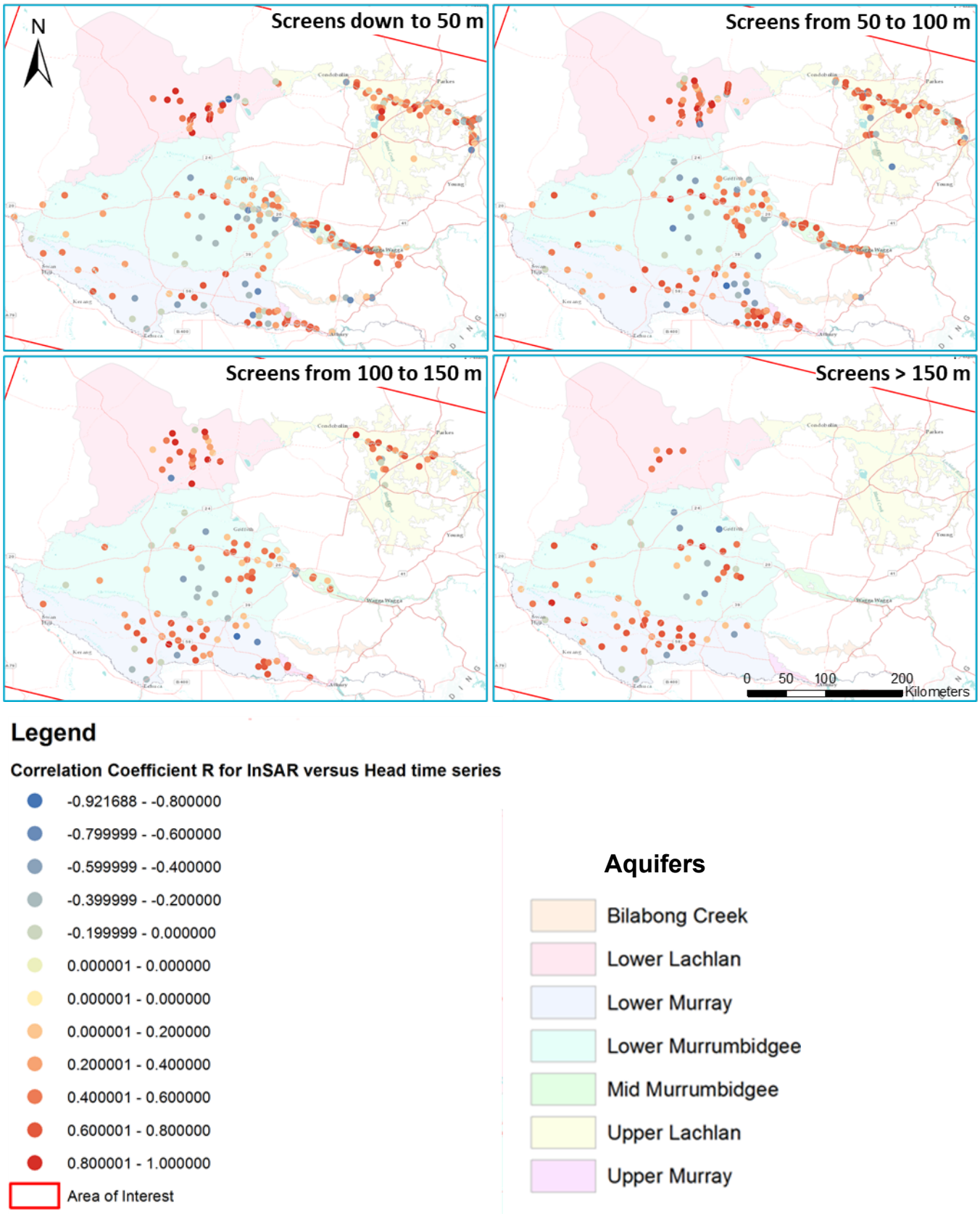

Figure 33 Horizontal and vertical distribution (by screen depths of bores) of positive and negative correlation between piezometric head and InSAR deformation time series.

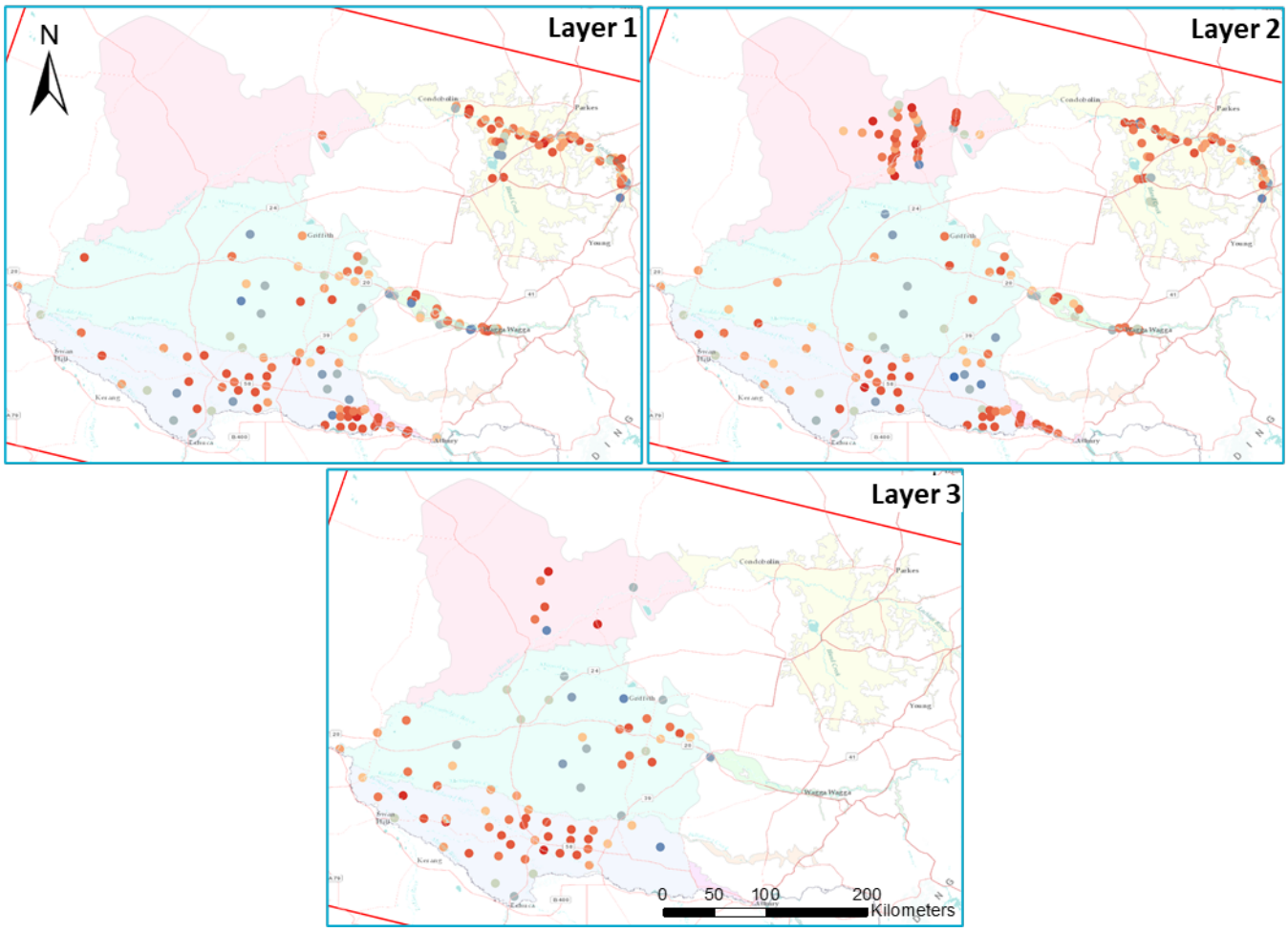

Legend

Correlation Coefficient R for InSAR versus Head time series

- -0.921688 - -0.800000
- -0.799999 - -0.600000
- -0.599999 - -0.400000
- -0.399999 - -0.200000
- -0.199999 - 0.000000
- 0.000001 - 0.000000
- 0.000001 - 0.000000
- 0.000001 - 0.200000
- 0.200001 - 0.400000
- 0.400001 - 0.600000
- 0.600001 - 0.800000
- 0.800001 - 1.000000
- Area of Interest

Aquifers

- Bilabong Creek
- Lower Lachlan
- Lower Murray
- Lower Murrumbidgee
- Mid Murrumbidgee
- Upper Lachlan
- Upper Murray

Figure 34 Horizontal and vertical distribution (by aquifer layers) of positive and negative correlation between piezometric head and InSAR deformation time series (layer attribution to bores derived from groundwater models).

6 Interpreting InSAR data using Machine Learning

This section describes the results of two efforts aimed at explaining the spatial variability of the temporal correlations between groundwater levels and ground deformation using a set of static or time-integrated covariates. For that purpose, we take advantage of the Random Forest method for its ability to provide insights about the hierarchical order of the covariates leading to an optimized explanatory model between behaviours of groundwater levels and ground levels for a set of wells, i.e., locations where groundwater level data are available. Inelastic deformation occurs when groundwater level reach unpresented minimums, leading to stress in the aquifer exceeding the pre-consolidation stress. In contrast, elastic deformation can occur with any groundwater level/pressure changes, regardless of the past level minimums or the pre-consolidation stress. First, we use a machine learning approach to explore the correlations indicative of inelastic deformation (InSAR vs. critical head time-series). Second, we use the same approach to explore the correlations indicative of elastic deformation (InSAR vs. head time-series).

6.1 Random Forest analysis

Random Forest (RF) is a machine learning algorithm, which was originally proposed by Ho (1995) and then further developed by Breiman (1996, 2001). It is a novel ensemble of classification and/or regression trees underpinned by bootstrapping subset selection technique, in which a model (or a tree) uses a random subset of the observations and controlling predictors to learn the pattern of the given data and attain the best prediction (Prasad et al., 2006; Vorpahl et al., 2012; Zamanirad et al., 2020). In other words, many trees (models) are constructed in a certain "random" way to form a Random Forest. The advantage of RF method is that it can reduce the correlation between decision trees by randomly selecting samples and features to overcome the overfitting issue of decision trees, thereby significantly improving the performance of the final model (Chen et al., 2020). Given its advantages, the RF has been widely used in practice from financial (such as bank industry, stock market) to healthcare and medicine sectors (such as breast cancer prediction), from e-commerce (such as price optimization) to professional sports (such as sports-related injury identification).

In the last a few years, several studies have used RF to investigate land subsidence and explore its associated factors. For example, Ilia et al. (2018) have used RF method to predict the subsidence deformation rate based on three variables, which can explain 75% variance based on the validation dataset, namely: thickness of loose deposits, the Sen's slope value of groundwater-level trend, and the Compression Index of the formation covering the area of interest.

Choubin et al. (2019) have predicted earth fissuring hazards, which is highly associated with land subsidence, with five machine learning models and found that the RF model was the best model in the modelling process. Sensitivity analysis indicated that the hazardous class was mainly related to low elevations with characteristics of high groundwater withdrawal, drop in groundwater level, high well density, high road density, low precipitation, and Quaternary sediments distribution.

Mohammady et al. (2019) assessed land subsidence susceptibility using random forest method and showed that distance from fault, elevation, slope angle, land use, and water table have the greatest impacts on subsidence occurrence.

Rahmati, et al. (2019) compared four tree-based machine learning models for land subsidence hazard modelling and concluded that the RF model had the lowest predictive error for mapping the LS hazard and the groundwater drawdown was seen to be the most influential factor that contributed to land subsidence in the study area.

Zamanirad et al. (2019) used three machine learning models (boosted regression trees (BRTs), generalized additive model (GAM), and random forest (RF)), to produce a spatial land subsidence-prone prediction map based on four anthropological and geo-environmental predictors. The RF model, as a benchmark model, showed slightly higher goodness of fit (85.45%) compared to the GAM, although its prediction power was lower than the GAM. The drawdown of groundwater level with 77.5% contribution was found to be the main causative predictor of land subsidence occurrence, followed by lithology (19.2%), distance from streams (2.5%), and altitude (0.8%).

Arabameri et al. (2020) evaluated 12 factor significance to land subsidence using a random forest (RF) model, and found that groundwater drawdown, land use and land cover, elevation, and lithology were the most important factors.

Chatrsimab et al. (2020) assessed the efficiency of hybrid algorithm Particle Swarm Optimization–Random forest (PSO-RF) for developing land subsidence prediction model with 11 factors. It was found that the media aquifer was the furthermost effective factor in the land subsidence development and followed by groundwater drawdown and transmissivity and storage coefficient.

Chen et al. (2020) have investigated the spatial correlation between Interferometric Synthetic Aperture Radar (InSAR) derived subsidence and groundwater levels in four aquifers in Beijing and concluded that the variation of groundwater level in the second confined aquifer has the strongest spatial correlation with subsidence in all the aquifers, although its impact has decreased after the South-to-North Water Diversion Project.

Ebrahimy et al. (2020) have produced and compared land subsidence susceptibility map using three machine learning approaches, i.e., the boosted regression tree (BRT), random forest (RF), and classification and regression tree (CART), with twelve influencing variables, namely altitude, slope angle, aspect, groundwater level, groundwater level change, land cover, lithology, distance to fault, distance to stream, stream power index, topographic wetness index, and plan curvature. The results showed that all the employed methods performed well, and the BRT model yielded slightly higher prediction accuracy than RF.

Elmahdy et al. (2020) have used RF model to spatially analyse the relationship between locations of land subsidence and sinkhole and conditioning factors (CFs) and showed that the area under the curve was 88.4%, for the RF model. The CFs include topographic factors (e.g., altitude, slope, topographic curvature), hydrological factors (palaeochannels and densities of palaeochannels), geological factors (surface and subsurface fault zones, distance from fault zones and lithological units) and land use/land cover (LULC) factors.

Arabameri et al. (2021) predicted the land subsidence distribution by generating land subsidence susceptibility models using five different artificial intelligence (AI) models and found the conditional random forest (Cforest) method yielded the best results.

In short, the RF technique has been used in the last decade to investigate the relationship between land subsidence derived from InSAR, remote sensing datasets, field surveys, and other

contributing factors. The main contributing factors vary from case study regions and local hydrogeological conditions.

6.2 Methodology and predictors

For this study, a multi-factorial RF analysis is used to explain the spatial variability in the relations between head behaviour and ground deformation. Note that the RF analysis here does not aim at predicting the spatial variability of InSAR deformation itself, but the variability in the relation between the temporal correlation coefficients calculated from InSAR deformation and critical head/groundwater level. The analysis uses a set of explanatory variables, sorted in four categories: surficial soils, terrain, groundwater and InSAR (Table 7). This analysis may provide some answers as to which predictors/variables have impact on spatially distributed temporal correlations between InSAR deformation and critical heads/groundwater levels over the observation period.

Table 7 List of the covariates used in the RF analysis.

Type of covariates	Acronym	Definition	Source
Surficial soils	Clay05	Fractional clay content for the soil layer 0-5cm	Soil and Landscape Grid Australia (Viscarra Rossel et al., 2014)
Surficial soils	Clay200	Fractional clay content for the soil layer 5-200cm	Soil and Landscape Grid Australia (Viscarra Rossel et al., 2014)
Surficial soils	SoilMoist.Trend	Trend in moisture content in 1st meter of soil	Australian Landscape Water Balance model (AWRA-L v6; Frost et al., 2018)
Surficial soils	SoiMoist.Mean	Mean moisture content in 1st meter of soil	Australian Landscape Water Balance model (AWRA-L v6; Frost et al., 2018)
Surficial soils	SoilMoist.Diff	Difference between mean moisture content in 1st meter of soil and the corresponding 2005-2015 mean value	Australian Landscape Water Balance model (AWRA-L v6; Frost et al., 2018)
Surficial soils	SoilMoist.Amp	Maximum amplitude of the moisture variations in 1st meter of soil	Australian Landscape Water Balance model (AWRA-L v6; Frost et al., 2018)
Surficial soils	Soil	Classification of soil types	Australian Soil Classification (ASC) soil type map of NSW
Terrain	Slope	Terrain slope	Calculated from ALOS-3D Digital Elevation Model (Tadono et al., 2016)
Terrain	Erodibility	Mean annual hillslope erosion (tonnes/ha/year) with C-factor	NSW-DPIE, Modelled Hillslope Erosion over New South Wales
Terrain	Dist.Stream	Euclidian distance to stream	Calculated from a map of perennial and major streams
Terrain	Elevation	Elevation in meters asl	ALOS-3D Digital Elevation Model (Tadono et al., 2016)

Table 7 (continued) List of the covariates used in the RF analysis.

Type of covariates	Acronym	Definition	Source
Groundwater	Screen.Depth	Depth of the screen for each well	NSW-DPIE
Groundwater	GWExtractionLayer1	Groundwater extraction in the upper aquifer	NSW-DPIE
Groundwater	GWExtractionLayer2	Groundwater extraction in the intermediary aquifer	NSW-DPIE
Groundwater	GWExtractionLayer3	Groundwater extraction in the deep aquifers	NSW-DPIE
InSAR	Inter.Perc	Percentage of quality interferograms	CSIRO - InSAR processing
InSAR	Spatial.CC	Mean spatial InSAR coherence, based on 150 randomly selected interferogram for each InSAR stacks.	CSIRO - InSAR processing
InSAR	Temp.CC	Temporal InSAR coherence, or 'stack' coherence	CSIRO - InSAR processing

The predictors used in the RF analysis analyse the overall value of each factor to predict the temporal correlation between InSAR deformation and critical head/groundwater level for the entire InSAR period and over the entire study area. That is, in contrast to the time-series correlation based on spatially distributed piezometers (Part II, section 5), the RF analysis uses static and time-integrated variables (totals, means, or trends for time-variable variables). As the analysis explained correlations between ground deformation and well information (groundwater levels and critical heads), it is dependent on such data and cannot lead to extrapolation beyond locations where the data is available.

6.3 Results

Temporal correlation between InSAR displacements and critical head time-series

The RF model of the temporal correlation between InSAR displacement and critical head including 18 predictors (Table 7) could explain 71.7% spatial variance, which is better than a linear regression model with the same 18 variables that could only explain 28.6% variance (R^2=0.286). The relative importance of RF (Figure 35) indicates that spatial InSAR coherence (Spatial.CC; a proxy for noise in InSAR data that is mainly caused by variations in land cover) and soil moisture (difference, trend, and amplitude) are the four most important factors resulting in a spatial pattern of correlation between InSAR displacements and critical head changes.

The left panel of Figure 35 shows the mean decrease in accuracy (%IncMSE) if we leave out a particular variable and the right panel shows the mean decrease in Mean Squared Error (MSE) (IncNodePurity), which is a measure of variable importance based on the Gini impurity index used for the calculating the splits in RF trees. The higher the value of mean decrease accuracy or mean decrease Gini score, the higher the importance of the variable in the model.

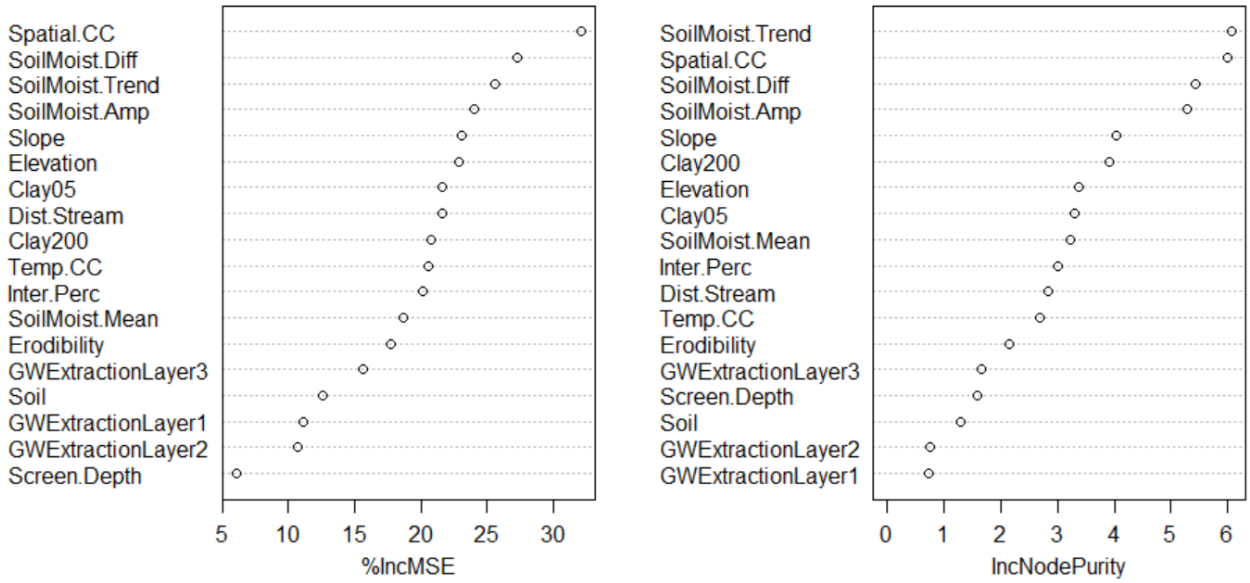

Figure 35 Relative importance of 18 predictors for the temporal correlation between InSAR displacement and critical head time-series.

An RF model with these four important factors was then build and it could explain 67.5% variance of spatial distribution of temporal correlation between InSAR displacements and critical head changes. This is almost the same as the full model with 18 predictors. Another RF model with only 3 soil moisture variables was also built and it could explain 65.2% spatial variance of temporal correlation between InSAR displacement and critical head. This is only slightly worse than the four-predictor model (-2.3%). This comparison is valid with the same random seed, given the "random" characteristics of RF method. This indicates that characteristics of soil moisture are critically important to explain the temporal correlations between InSAR displacement and critical head. However, it seems the RF model slightly underpredicts the positive correlation values between InSAR displacement and critical heads and overpredicts the negative correlation values (Figure 36). The 3-predictor model was then run 1000 times to quantify the random characteristics of RF method and it shows that it is a robust model having a variance explained below 65.0–67.9% (Figure 37).

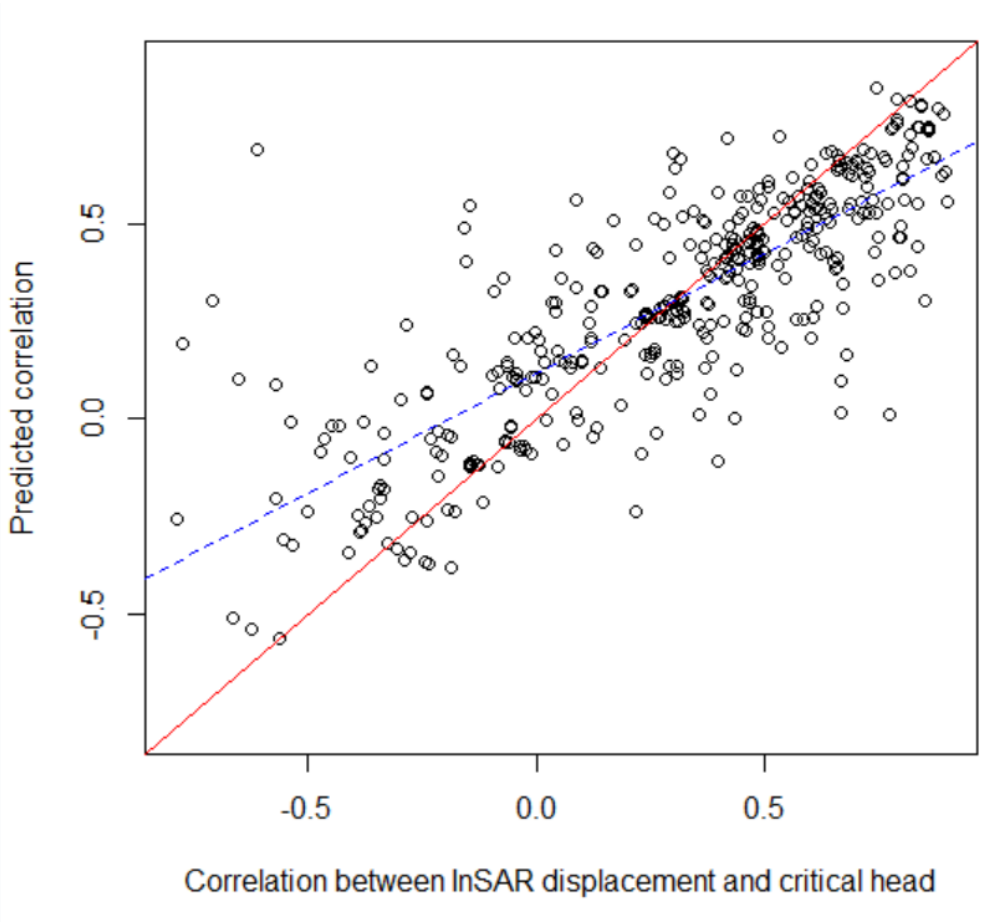

Figure 36 Correlation between InSAR displacement and critical head vs RF simulated results (red line is the 1:1 line and blue dash line is the linear fitted line).

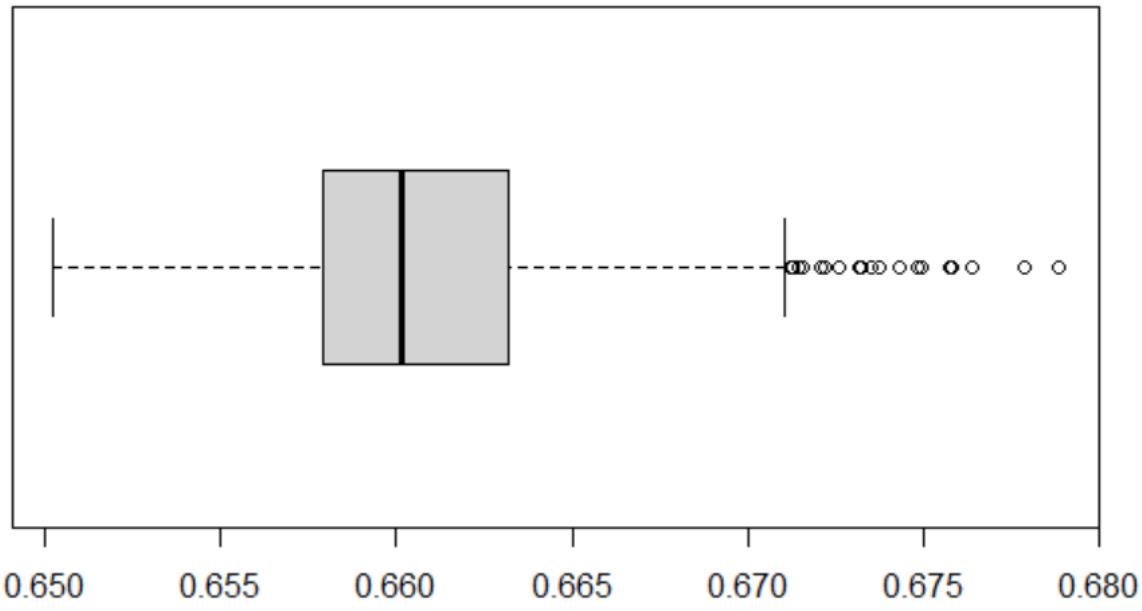

Figure 37 Variance explained with 3-predictor RF model of correlation between InSAR displacement and critical head (1000 runs).

Temporal correlation between InSAR displacement and groundwater level time-series

The RF model of the temporal correlation between InSAR displacement and groundwater level including 18 predictors could explain 60.0% spatial variance, which is also much better than a linear regression model with the same 18 variables that could only explain 9.7% variance (R^2=0.097). These two values are both lower than their corresponding values between InSAR displacements and critical heads, i.e., 71.7% vs 60.0% and 28.6% vs 9.7%.

The relative importance of RF (Figure 38) indicates that temporal and spatial InSAR coherence (Temp.CC and Spatial.CC; both are proxy for noise in InSAR data that is mainly caused by variations in land cover) and soil moisture (difference, trend and amplitude) are the most important factors resulting in a spatial pattern of correlation between InSAR displacements and groundwater heads. However, it is noted that different rankings for variable importance could be obtained based on two different criteria. For example, screen depth of a bore (Screen.Depth) is the second important variable to explain the spatial variance of correlation between InSAR displacements and groundwater levels based on IncNodePurity, but it is only ranked 10th out of 18 variables based on %IncMSE (Figure 38). In theory, there is no fixed criterion to select the "best" measure of variable importance.

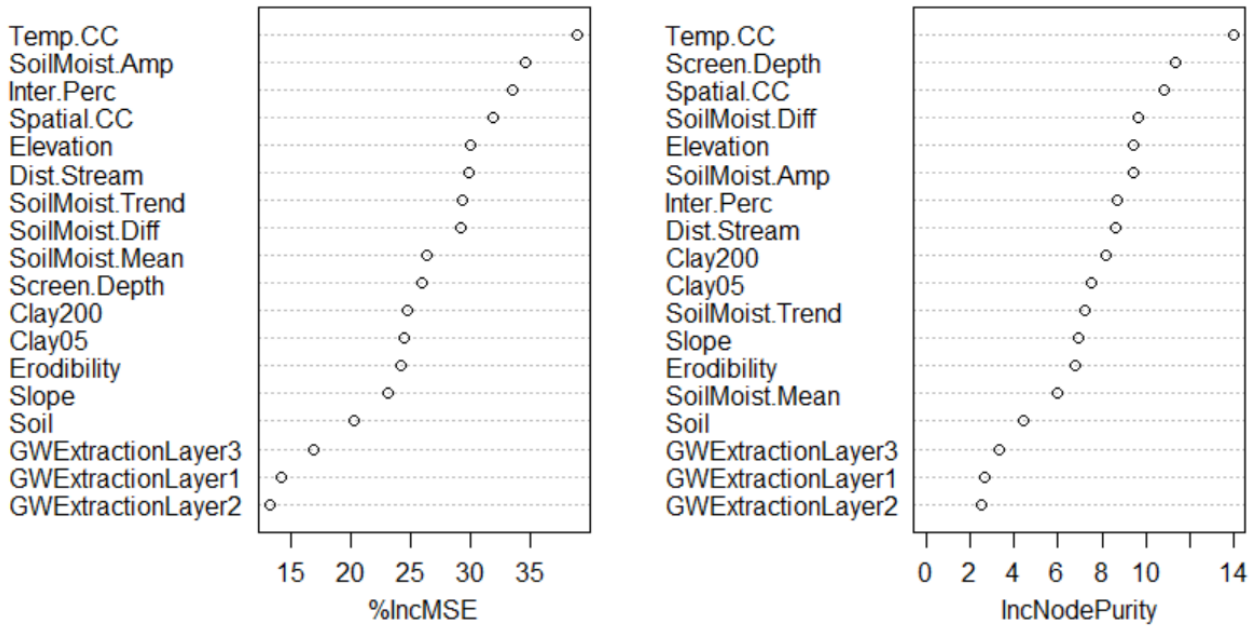

Figure 38 Relative importance of 18 predictors for the temporal correlation between InSAR displacement and groundwater level time-series.

6.4 Interpretation and Perspectives

One RF model is produced jointly for all aquifers, with lithological heterogeneity largely unaccounted in the set of covariates (Table 7). This leads to an inherent underestimation of the influence of groundwater factors in the RF analysis. Nevertheless, a competent model with R^2>0.7 can be build using the proposed set of covariates, which reinforce the idea that both surficial soils and InSAR noise (due to land use and artefacts of deformation model fitting) are important contributing factors in the InSAR results, thus in its temporal correlation with groundwater level changes. More generally, we note that the RF machine learning technique is useful to investigate

the spatial distribution of correlation between InSAR and critical head/groundwater level, and their contributing factors.

The RF model was run based on monitoring bore locations only because we target the temporal correlation between InSAR displacement and critical head/groundwater level. The results indicate that soil moisture variables (3 statistics) are most important to explain the spatial variance of temporal correlation between InSAR displacement and critical head. If the relationships between the soil moisture and temporal correlation can be explained as a physically based processes, then the spatial distribution of temporal correlation could be predicted with the soil moisture and the RF model. Given the potentially serious damages to farms and urban infrastructure and other environmental issues that land subsidence could cause, a prediction model could be useful for practical applications.

The RF model could also be run for each individual year (5-year data implies five different RF models) because the hydroclimate conditions vary from year to year or each groundwater management area, which could tell us whether the most important contributing factors are the same or different within a wet/dry year and a different groundwater management area. More importantly, the RF model could be run for each individual aquifer, which would help the model account for lithological variability, given that the latter is potentially less heterogenous at the aquifer-scale rather than at the scale of the entire study area.

Conclusion

For the period from November 2015 to May 2020, InSAR detects background deformation rates over most of the study area, with values in the range [-10; 10] mm/yr. However, some anomalies beyond this range are detected, and two of them are potentially related to groundwater extraction. First, the Murray catchment presents a spatially distributed uplift signal, it is not spatially continuous and follows agricultural boundaries, suggesting that the signal is unrelated to groundwater, and potentially more related to a series of soil surface deformations and vegetation-related noise in InSAR deformation data. Second, four main, low amplitude, negative deformation areas (land subsidence) are potentially attributable to groundwater extraction: the Darlington Point area, also encompassing the Coleambally area (eastern Lower Murrumbidgee groundwater source) shows subsidence rates in the range [-10; -30] mm/yr. The Hillston area (eastern Lower Lachlan groundwater source) and the river corridors in the Upper Lachlan and Upper Murray also show rates of similar amplitude. Given the low amplitude of such deformation and its spatial patterns not clearly coinciding with any obvious geomorphological or lithological boundaries, allocating the deformation to specific phenomena (e.g., groundwater depletion and storage, surface water and flooding, agricultural activities, soil clay content, climate variations to name a few) requires a multi-line of evidence approach. Table 8 lists the main deformation anomalies detected over each aquifer during the InSAR observation period and provides a qualitative assessment of the potential for groundwater to be the main contributing factor for inelastic compaction during this period.

A temporal correlation method is first used to explore the potential causal effects between groundwater and ground level changes. Time series of InSAR-derived displacement in localised areas and at certain aquifer depths were confirmed to be strongly correlated with critical head drop, i.e., dewatering that causes consolidation. Examples of these localised areas and their affected aquifer depths are, e.g., the eastern Lower Murrumbidgee and the eastern Lower Lachlan in the deeper aquifers (within the Calivil and Renmark formations) and along the river corridors of the Upper Lachlan and Upper Murray in the shallower aquifers (within the Cowra/Shepparton and Lachlan formations). Note that groundwater levels in the Mid Murrumbidgee and Lower Murray did not exceed historic minima established prior to the InSAR observation period. Hence, in these areas no new critical heads were available for any correlation with InSAR deformation.

In contrast to the spatial clustering of piezometers with good critical head-vs-InSAR-correlation in anomaly areas, piezometers with strong correlations between groundwater level oscillations and InSAR displacement time series are more widespread and denser and suggestive of elastic compaction and expansion. However, strong head vs InSAR correlations in each area occur mostly at the same aquifer depths as described above for the compaction observed during critical head drop periods. Thus, while the relation between ground deformation is obvious for certain areas, it is impossible to conclude on the elastic or inelastic nature of the ground deformation.

Table 8 Summary of the ground deformation anomalies and assessment of their potential relation to groundwater.

Aquifer	Deformation anomalies	Anomaly areas coincide with groundwater extraction	Significant correlation either with groundwater level hydrographs or with critical head			Potential for groundwater-induced inelastic compaction
			Groundwater hydrographs	Critical head drop	Affected formation	
Lower Lachlan	Up to -25 mm/yr in the corridor between the Lachlan river and Merrowie Creek near Hillston	Yes	Yes	Yes	Calvil and Remark	High
	Up to -20 mm/yr around and North of Wilandra National Park	No	No	No	-	Low
Lower Murrumbidgee	Up to -20 mm/yr around Coleambally and Darlington Point	Yes	Yes	Yes	Calvil and Renmark	High
	Up to -25 mm/yr at the western end of the aquifer, around the Murrumbidgee River	No	No	No	-	Low
Lower Murray	Sparse signals in the range [-25; -10] mm/yr in the centre near Finley	No	Yes	No	All layers (but only for elastic deformation)	Low (only correlation with ground-water heads, but not critical heads)
	Sparse signals in the range [-25; -10] mm/yr towards the western part of the aquifer	No	No	No	-	Low
Upper Lachlan	Up to -15 mm/yr sparsely distributed mainly along the river corridor	Yes	Yes	Yes	Cowra and Lachlan	Medium
	Up to -15 mm/yr sparsely distributed in the area of Garema	No	No	No	-	Low
Mid-Murrumbidgee	Up to -10 mm/yr sparsely distributed	Yes	Yes	No	-	Low
Billabong Creek	None	No	No	No	-	Low
Upper Murray	Up to -15 mm/yr sparsely distributed	Yes	Yes	Yes	Shepparton and Lachlan	Low

These time-series correlation analyses were only conducted as single variable regression analyses, and as such, are not multivariate correlation analyses. The weak correlations in many bore locations suggests that other non-groundwater, surface-related parameters are at play. This was confirmed by two multi-factorial 'Random Forest' analyses aimed at explaining the spatial variability in the relations between head behaviour and ground deformation. Note that these analyses do not aim at explaining the spatial variability of ground deformation itself, but of the relation between ground deformation and critical head drop that can cause inelastic subsidence and of the relation between ground deformation and groundwater level oscillations that can cause elastic compaction/expansion. While 18 variables were used, the groundwater factors were largely underrepresented, leading to an inherent underestimation of the influence of groundwater level changes on ground deformation. However, two important observation are drawn from this analysis: (1) an accurate model can be built using that dataset; (2) surficial soil deformation and InSAR noise parameters are highly ranked in the hierarchical order of influential covariates for the model. This means that, when considering the entire study area (seven alluvial aquifers), critical head is not an influential predicator of the ground deformation. This is somewhat expected given that lithological parameters, which usually explain the spatial variations of the groundwater-ground levels reaction, are unaccounted. This inherently increases the relative importance of other parameters. Nevertheless, such result confirms that deformation from surficial soils (clay content, moisture changes) should be accounted while interpretating InSAR data. InSAR measurement noise cannot be avoided given the wavelength of the radar data available over the study area but will improve in the near future with the expected availability of longer wavelength radar data.

Future work could focus on pushing some limitation of this study or on taking advantage of upcoming radar missions.

First, the relation between ground deformation and groundwater could be further explored by:

- Placing corner reflectors (specifically designed ground targets reflecting the radar signal) over locations where ground deformation and groundwater levels (and in particular critical heads) are highly correlated and where groundwater depletion occurs. This would largely increase the precision of the ground deformation data and potentially prevent most of the influence from surficial clays.
- Performing improved "child" Random Forest analyses, designed similarly to the one presented in this study, but focusing on certain areas where lithological information is available and can be accounted for (fine-grained content per aquifer, aquifer/aquitard thickness etc). The Random Forest analysis would therefore be completer and more balanced, with all potential explanatory factors well represented by covariates. It is expected that compilation of consistent lithological information is more available on the basis of individual groundwater sources or even, on a more local scale, in areas of piezometer-clusters that show similar strong positive temporal correlation between critical heads and InSAR deformation.

Second, and more generally, a better allocation of ground deformation data to influential factors is an important science gap to fill for any future interpretation of ground deformation data in Australia, including groundwater applications. This challenge can be tackled by:

- Comparing SBAS-InSAR ground deformation data influenced by surficial clays with InSAR analysis targeted on highly coherent radar targets unaffected by surficial clays (house, buildings, or comer reflectors).
- Measuring in-situ the surficial ground deformation and its relation to moisture and cropping cycles, in the perspective of correcting InSAR deformation maps for its non-groundwater contributors.

References

Ali A, Merrick NP, Williams RM, Mampitiya D, d'Hautefeuille F, Sinclair P (2004) Land settlement due to groundwater pumping in the Lower Namoi Valley of NSW. In Proceedings of 9th Murray Darling Basin Groundwater Workshop, Bendigo, Australia.

Arabameri A, Saha S, Roy J, Tiefenbacher JP, Cerda A, Biggs T, Pradhan B, Ngo PT, Collins AL (2020) A novel ensemble computational intelligence approach for the spatial prediction of land subsidence susceptibility. Science of The Total Environment, 726. DOI:10.1016/j.scitotenv.2020.138595

Arabameri A, Pal SC, Rezaie F, Chakrabortty R, Chowdhuri I, Blaschke T, Ngo PT (2021) Comparison of multi-criteria and artificial intelligence models for land-subsidence susceptibility zonation. J Environ Manage, 284. DOI:10.1016/j.jenvman.2021.112067

Berardino P, Fornaro G, Lanari R, Sansosti E (2002) A new algorithm for surface deformation monitoring based on small baseline differential SAR interferograms. IEEE Trans. Geosci. Remote Sens. 40, 2375–2383. DOI:10.1109/TGRS.2002.803792

Breiman L (1996) Bagging predictors. Mach. Learn. 24, 123–140. DOI:10.1007/ BF00058655.

Breiman L (2001). Random forests. Mach. Learn. 45, 5–32. DOI:10.1023/A: 1010933404324.

Castellazzi P, Schmid W (2020) Ground displacements in the Lower Namoi region. NSW DPIE: CSIRO; 2020. http://hdl.handle.net/102.100.100/367006?index=1

Castellazzi, P, Schmid, W (2021) Interpreting C-band InSAR ground deformation data for large-scale groundwater management in Australia. J. Hydrol. Reg. Stud. 34, 100774. DOI: 10.1016/j.ejrh.2021.100774

Chatrsimab Z, Alesheikh AA, Voosoghi B, Behzadi S, Modiri M (2020) Development of a Land Subsidence Forecasting Model Using Small Baseline Subset-Differential Synthetic Aperture Radar Interferometry and Particle Swarm Optimization-Random Forest (Case Study: Tehran-Karaj-Shahriyar Aquifer, Iran). Doklady Earth Sciences, 494(1): 718-725. DOI:10.1134/s1028334x20090056

Chen B, Gong H, Chen Y, Li X, Zhou C, Lei K, Zhu L, Duan L, Zhao X (2020) Land subsidence and its relation with groundwater aquifers in Beijing Plain of China. Science of the Total Environment, 735. DOI:10.1016/j.scitotenv.2020.139111

Choubin B, Mosavi A, Alamdarloo EH, Hosseini FS, Shamshirband S, Dashtekian K, Ghamisi P (2019) Earth fissure hazard prediction using machine learning models. Environmental Research, 179. DOI:10.1016/j.envres.2019.108770

Ebrahimy H, Feizizadeh B, Salmani S, Azadi H (2020) A comparative study of land subsidence susceptibility mapping of Tasuj plane, Iran, using boosted regression tree, random forest and classification and regression tree methods. Environmental Earth Sciences, 79(10). DOI:10.1007/s12665-020-08953-0

Elmahdy SI, Mohamed MM, Ali TA, Abdalla JE, Abouleish M (2020) Land subsidence and sinkholes susceptibility mapping and analysis using random forest and frequency ratio models in Al Ain, UAE. Geocarto International. DOI:10.1080/10106049.2020.1716398

Frost AJ, Ramchurn A, Smith A (2018) The Australian Landscape Water Balance Model. Bureau of Meteorology: Melbourne, Australia.

Ho TK (1995) Random decision forests. In Proceedings of 3rd international conference on document analysis and recognition (Vol. 1, pp. 278–282). IEEE.

Ilia I, Loupasakis C, Tsangaratos P (2018) Land subsidence phenomena investigated by spatiotemporal analysis of groundwater resources, remote sensing techniques, and random forest method: the case of Western Thessaly, Greece. Environmental Monitoring and Assessment, 190(11). DOI:10.1007/s10661-018-6992-9

Mathevet T, Gupta H, Perrin C, Andreassian V, Le Moine N (2020) Assessing the performance and robustness of two conceptual rainfall-runoff models on a worldwide sample of watersheds. Journal of Hydrology, 585. DOI:10.1016/j.jhydrol.2020.124698

Mohammady M, Pourghasemi HR, Amiri M (2019) Land subsidence susceptibility assessment using random forest machine learning algorithm. Environmental Earth Sciences, 78(16). DOI:10.1007/s12665-019-8518-3

NSW (2021a) Water Resource Plans. https://www.industry.nsw.gov.au/water/plans-programs/water-resource-plans accessed 29/06/2021

NSW (2021b) Water Sharing Plans. https://www.industry.nsw.gov.au/water/plans-programs/water-sharing-plans\ accessed 29/06/2021

Prasad AM, Iverson LR, Liaw A (2006) Newer classification and regression tree techniques: Bagging and random forests for ecological prediction. Ecosystems, 9(2), 181–199

Rahmati O, Falah F, Naghibi SA, Biggs T, Soltani M, Deo RC, Cerdà A, Mohammadi F, Bui DT (2019) Land subsidence modelling using tree-based machine learning algorithms. Science of the Total Environment, 672: 239-252. DOI:10.1016/j.scitotenv.2019.03.496

Sowter A, Bateson L, Strange P, Ambrose K, Syafiudin MF (2013) DInSAR estimation of land motion using intermittent coherence with application to the South Derbyshire and Leicestershire coalfields. Remote Sens. Lett. 4, 979–987. https://doi.org/10.1080/2150704X.2013.823673

Tadono T, Nagai H, Ishida H, Oda F, Naito S, Minakawa K, Iwamoto H (2016) Generation of the 30 M-Mesh Global Digital Surface Model by Alos Prism. International Archives of the Photogrammetry, Remote Sensing & Spatial Information Sciences. 2016 Jul 15;41.

Viscarra Rossel R, Chen C, Grundy M, Searle R, Clifford D and Odgers N (2014) Soil and landscape grid Australia-Wide 3D Soil Property Maps (3 ”resolution)–release 1. v2. CSIRO, http://www.clw.csiro.au/aclep/soilandlandscapegrid/index.html.

Vorpahl P, Elsenbeer H, Märker M, Schröder B (2012) How can statistical models help to determine driving factors of landslides?. Ecological Modelling. 2012 Jul 24; 239: 27-39.

Zamanirad M, Sarraf A, Sedghi H, Saremi A, Rezaee P (2020) Modeling the Influence of Groundwater Exploitation on Land Subsidence Susceptibility Using Machine Learning

Algorithms. Natural Resources Research, 29(2): 1127-1141. DOI:10.1007/s11053-019-09490-9

WMA (2000) Water Management Act 2000 (NSW) s. 324, retrieved from https://www.legislation.nsw.gov.au/#/view/act/2000/92/chap7/part1/div2/sec324

CONTACT US

t 1300 363 400
+61 3 9545 2176
e csiroenquiries@csiro.au
w www.csiro.au

AT CSIRO, WE DO THE EXTRAORDINARY EVERY DAY

We innovate for tomorrow and help improve today – for our customers, all Australians and the world.

Our innovations contribute billions of dollars to the Australian economy every year. As the largest patent holder in the nation, our vast wealth of intellectual property has led to more than 150 spin-off companies.

With more than 5,000 experts and a burning desire to get things done, we are Australia's catalyst for innovation.

CSIRO. WE IMAGINE. WE COLLABORATE. WE INNOVATE.

FOR FURTHER INFORMATION

LAND AND WATER
Wolfgang Schmid
t +61 8 9333 6793
e wolfgang.schmid@csiro.au

FOR FURTHER INFORMATION

LAND AND WATER
Pascal Castellazzi
t 61 4 5237 2066
e pascal.castellazzi@csiro.au